1981

An upper limit for the methane-oxygen initation reaction in the presence of iodine-131 behind reflected shock waves

Steven Peter Pardini
Iowa State University

Pardini, Steven Peter

AN UPPER LIMIT FOR THE METHANE-OXYGEN INITIATION REACTION IN THE PRESENCE OF IODINE-131 BEHIND REFLECTED SHOCK WAVES

Iowa State University PH.D. 1981

PLEASE NOTE:

In all cases this material has been filmed in the best possible way from the available copy. Problems encountered with this document have been identified here with a check mark ✓.

1. Glossy photographs or pages _____
2. Colored illustrations, paper or print _____
3. Photographs with dark background ✓
4. Illustrations are poor copy _____
5. Pages with black marks, not original copy _____
6. Print shows through as there is text on both sides of page _____
7. Indistinct, broken or small print on several pages ✓
8. Print exceeds margin requirements _____
9. Tightly bound copy with print lost in spine _____
10. Computer printout pages with indistinct print _____
11. Page(s) _____ lacking when material received, and not available from school or author.
12. Page(s) _____ seem to be missing in numbering only as text follows.
13. Two pages numbered _____. Text follows.
14. Curling and wrinkled pages _____
15. Other _____

An upper limit for the methane-oxygen initiation reaction in the presence of iodine-131 behind reflected shock waves

by

Steven Peter Pardini

A Dissertation Submitted to the
Graduate Faculty in Partial Fulfillment of the
Requirements for the Degree of
DOCTOR OF PHILOSOPHY

Department: Chemistry
Major: Physical Chemistry

Approved:

Signature was redacted for privacy.

In Charge of Major Work

Signature was redacted for privacy.

For the Major Department

Signature was redacted for privacy.

For the Graduate College

Iowa State University
Ames, Iowa

1981

TABLE OF CONTENTS

DEDICATION

To my mother, father and brother,
all of whom I love dearly.

INTRODUCTION

> "One of the very important aspects of the kinetic art, and it is still an art, is the dissection of an observed rate into the rate constants for elementary molecular steps." (1)

This work is a study of methyl-radical formation and kinetics that is related to the general problem of the initiation of methane combustion.

Methane Combustion Overview

Even methane, the simplest of all hydrocarbons, involves a combustion chain process which is exceedingly complex, a chain which must not only include C_1 and C_2 carbon pathways, but must also involve formaldehyde, hydrogen and carbon monoxide oxidation as well.

Elucidation of the chemical process involved in the combustion of methane requires accurate kinetic data on the elementary molecular steps.

Current experimental determinations of elementary rate constants are providing needed modification and updating of information on methane combustion. Developments which recently have had major implications for combustion chemistry are: determination of the properties of elementary reactions and hence their rate constants (2), determination of the curvature in Arrhenius graphs over large temperature ranges (3), and determination of the density dependence of dissociation-recombination reactions (4).

The study of individual reaction steps in separate experiments must be performed to achieve major progress in future understanding of

reaction mechanisms of methane combustion. Data of this type coupled with the simultaneous, single-experiment measurement of concentration-time profiles of the many species present during the oxidation process would help to achieve a coherent and integrated description of the complex methane-oxygen combustion reaction.

Ignition-time studies on methane-oxygen-argon mixtures from shock-tube experiments are conveniently described by Equation [1],

$$\tau = A[CH_4]^{\alpha}[O_2]^{\beta}[Ar]^{\gamma}\exp(E/RT) \qquad [1]$$

where the parameters α, β, γ and E are found by judicious combination of experimental data and theoretical calculations. The relationship of Equation [1] to the mechanism of methane oxidation is not immediately obvious. Ignition-time studies alone are useful for some applications, but from data of this type it is difficult to determine individual rate constants regarding doubtful reactions, and it is difficult to deduce information regarding overall mechanisms.

Validation of adopted rate constants and postulated mechanisms requires the use of ignition-time data, accurate values of pertinent elementary reactions and the comparison of calculated and observed concentration-time profiles. Numerous ignition-time studies have been performed and many of the important elementary-reaction rate constants are known. Concentration-time profiles have been calculated by many authors using various mechanisms and modeling techniques, but experimentally measured concentration-time histories are unavailable for many species known to exist during the combustion process. The current

published concentration-time profiles data rarely refer to a single experiment, recorded intensities are rarely reduced to absolute concentrations, signal-to-noise ratios are quite low, and quenched reaction mixture samples cover a limited range of reaction conditions and a limited number of species. There is still much to be done in the study and analysis of methane-oxygen combustion.

The process of methane oxidation may be divided into two periods: the induction period and the main reaction period. The induction period may be subdivided into two phases: the initiation phase and the chain-branching phase. The main reaction period also consists of two phases: the methane-consumption phase and the carbon monoxide-oxidation phase.

A methane-oxygen shock-tube-ignition experiment performed by Tsuboi and Wagner (5) at 1600 K on a 0.2% methane 2% oxygen mixture diluted in argon at a total density of 1.8×10^{-4} moles/cm^3 was found to have an induction period of nearly 200 μs and a main-reaction period of approximately 50 μs. During the induction period, less than 10% of the methane was consumed, and a minimal amount of reaction heat was evolved. In the main reaction period, a rapid pressure and temperature increase occurred, and the methane concentration dropped essentially to zero.

Westbrook (6) carried out an analytical study of the ignition of methane using a numerical model consisting of 25 reaction species and 75 elementary reactions. A calculated induction time of 270 μs at 1500K for a stoichiometric methane-oxygen mixture diluted in argon at 9.5×10^{-5} moles/cm^3 was found to be in good agreement with experimental results. A tabulation of the concentrations of the principal radical species was made at 25 μs of reaction time, and is shown in Table 1.

Table 1. Selected radical-species' concentrations at 25 μs of reaction time at 1500K

Species	Concentration (moles/cm^3)
H	5.7×10^{-12}
O	3.7×10^{-11}
OH	5.1×10^{-12}
HO_2	1.9×10^{-10}
CH_3	3.9×10^{-9}

Radical-species' concentrations increased rapidly during the initiation phase, and varied slowly during the chain-branching phase. In this study, the principal radical species, (H, O, OH, HO_2) had already risen to their respective steady-state concentration levels at 25 μsec; thus, Westbrook's results indicated that the initiation phase was very short compared to the chain-branching phase.

The initiation phase is characterized mainly by the thermal decomposition of methane Reaction (1)

$$CH_4 + M \rightleftarrows CH_3 + H + M. \qquad (1)$$

The direct attack on methane by oxygen in Reaction (2)

$$CH_4 + O_2 \rightleftarrows CH_3 + HO_2 \qquad (2)$$

and the dissociation of oxygen molecules in Reaction (3)

$$O_2 + M \rightleftarrows O + O + M \qquad (3)$$

has been supported by various experiments as probable initiation steps. Although a direct experimental determination of Reaction (2) has not been reported, this reaction is believed by some authors (7,8) to be of greater importance than Reaction (1) below 1700K. Reaction (3) had been found to occur above 2000K in highly diluted reaction mixtures, by Glass et al. (9).

The principal product of the initiation phase is the methyl radical. The slow reactions of the methyl radical lead to the formation and rapid build up of a radical pool. These radical species, particularly H, O, OH and HO_2, accelerate methane consumption and lead to the formation and consumption of intermediate products, viz., H_2, CH_2O, CO, C_2H_6, C_2H_4, C_2H_2 and to the formation of H_2O, during the chain-branching phase.

The reaction of oxygen with methyl radicals is of considerable importance during the early stages of the chain-branching phase. Reaction (4)

$$CH_3 + O_2 \rightleftarrows CH_2O + OH \qquad (4)$$

results in the formation of formaldehyde and hydroxyl radical. This reaction is expected to dominate at lower temperatures over Reaction (5)

$$CH_3 + O_2 \rightleftarrows CH_3O + O \qquad (5)$$

which has a larger activation energy. The methoxy radical formed in Reaction (5) decomposes to yield formaldehyde and hydrogen atom via Reaction (6)

$$CH_3O + M \rightleftarrows CH_2O + H + M \; . \qquad (6)$$

Formaldehyde is involved in a degenerate-branching reaction with argon atoms in Reaction (7)

$$CH_2O + M \rightleftarrows HCO + H + M \ . \qquad (7)$$

In the final stages of the chain-branching phase, formaldehyde reactions with hydrogen and oxygen atoms and hydroxyl and hydroperoxyl radicals via Reactions (8), (9), (10) and (11)

$$CH_2O + H \rightleftarrows HCO + H_2 \qquad (8)$$

$$CH_2O + O \rightleftarrows HCO + OH \qquad (9)$$

$$CH_2O + OH \rightleftarrows HCO + H_2O \qquad (10)$$

$$CH_2O + HO_2 \rightleftarrows HCO + H_2O_2 \qquad (11)$$

dominate formaldehyde oxidation. Formyl radical decomposition via Reaction (12)

$$HCO + M \rightleftarrows CO + H + M \qquad (12)$$

leads to the formation of carbon monoxide and hydrogen atoms.

The hydroxyl radical is highly reactive and responsible for most of the methane consumption via Reaction (13)

$$CH_4 + OH \rightleftarrows CH_3 + H_2O \ , \qquad (13)$$

yet it is not involved in branching reactions. Hydrogen and oxygen atoms are involved in branching reactions and make a significant contribution to bimolecular-abstraction reactions responsible for methane consumption via Reactions (14) and (15)

$$CH_4 + H \rightleftarrows CH_3 + H_2 \qquad (14)$$

$$CH_4 + O \rightleftarrows CH_3 + OH \ . \qquad (15)$$

The hydroperoxyl radical may also contribute to methane consumption through Reaction (16)

$$CH_4 + HO_2 \rightleftarrows CH_3 + H_2O_2 \ . \qquad (16)$$

In a lean mixture above 1700K, the formation of hydrogen through Reaction (14) occurs to a lesser extent than hydrogen-atom attack on oxygen molecules via Reaction (17)

$$H + O_2 \rightleftarrows OH + O \ . \qquad (17)$$

Additional hydrogen-oxygen combustion reactions are of importance during the branching phase of the induction period. Reactions (18), (19), (20) and (21)

$$O + H_2 \rightleftarrows OH + H \qquad (18)$$

$$H + H_2O \rightleftarrows OH + H_2 \qquad (19)$$

$$O + H_2O \rightleftarrows OH + OH \qquad (20)$$

$$H + O_2 + M \rightleftarrows HO_2 + M \qquad (21)$$

are several examples.

The methyl-radical concentration is limited by a large number of reactions, but by far the most important of these reactions is the recombination of methyl radicals in Reaction (22)

$$CH_3 + CH_3 \ (+M) \rightleftarrows C_2H_6 \ (+M) \ . \qquad (22)$$

This reaction is responsible for the consumption of a substantial fraction of the methyl radicals even in oxygen-rich reaction mixtures.

Westbrook (6) demonstrated experimentally and by computer modeling the effect of the creation and oxidation of ethane (along with ethylene and acetylene) on the length of ignition time. Thus, these species and their reactions were included in the reaction scheme in order to explain induction-time phenomena accurately.

The largest contributor to ethane loss came from Reaction (23)

$$C_2H_6 + H \rightleftarrows C_2H_5 + H_2 \quad . \tag{23}$$

The ethyl radical formed in Reaction (23) decomposed via Reaction (24)

$$C_2H_5 \ (+M) \rightleftarrows C_2H_4 + H \ (+M) \tag{24}$$

yielding ethene and a hydrogen atom. Westbrook believed that ethene consumption occurred through two major pathways. Approximately half of the ethene produced vinyl radicals and water through Reaction (25)

$$C_2H_4 + OH \rightleftarrows C_2H_3 + H_2O \tag{25}$$

and the other half produced methyl and formyl radicals through Reaction (26)

$$C_2H_4 + O \rightleftarrows HCO + CH_3 \quad . \tag{26}$$

In Reaction (27)

$$C_2H_3 + M \rightleftarrows C_2H_2 + H + M \tag{27}$$

ethyl radicals decomposed yielding acetylene and a hydrogen atom. Acetylene reacted primarily with oxygen through Reaction (28)

$$C_2H_2 + O \rightleftarrows CH_2 + CO \quad . \tag{28}$$

The CH_2, C_2H and CH species reacted rapidly producing the formyl radical and carbon monoxide.

In a review article on high-temperature combustion by Gardiner and Olson (10), Figure 1 was given as a simplified flow diagram of elementary reactions interrelating small-hydrocarbon systems. Differences between the work of Westbrook (6) and Olson and Gardiner's flow diagram on C_2 carbon chemistry may be compared.

The main feature of the induction period is the growth of the methyl radical over many orders of magnitude. The concentrations of hydrogen and oxygen atoms, hydroxyl, hydroperoxyl and methoxy radicals are in a quasi-steady state in the sense that the rate of creation and consumption very nearly cancel although concentrations do vary slowly. As the methyl-radical concentration increases, the other radical concentrations rise proportionately and the reaction rate increases in response to the radical concentration rise. The induction period ends when the reaction rates become large enough to cause a rapid increase in temperature and pressure. Rate constants for the induction period reactions are found in Table 2. By no means are the reactions presented here to be considered as an all-inclusive mechanistic set.

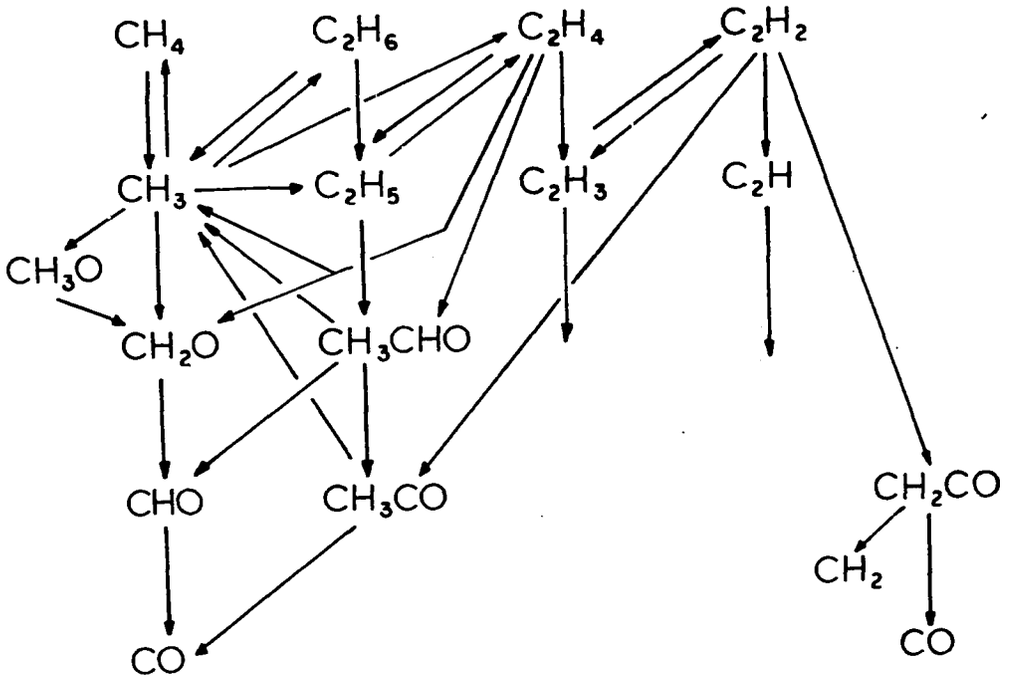

Figure 1. Flow diagram illustrating oxidation routes of small hydrocarbons as far as to CO and H_2. The intermediates H, O, OH, and M and the product H_2O are omitted for clarity. Also not shown are the reactions of C_2H, C_2H_3 and CH_2. From reference (10)

Table 2. Induction-period rate constants for forward reactions $k = AT^n\exp(-E/RT)$ in cm^3, mole, sec, kcal units

Reaction	log A	n	E	Reference
1. $CH_4 + M \rightleftarrows CH_3 + H + M$	17.3	0	88.4	11
2. $CH_4 + O_2 \rightleftarrows CH_3 + HO_2$	13.9	0	56.0	7
3. $O_2 + M \rightleftarrows O + O + M$	15.48	0	124.0	12
4. $CH_3 + O_2 \rightleftarrows CH_2O + OH$	11.84	0	9.00	13
5. $CH_3 + O_2 \rightleftarrows CH_3O + O$	13.4	0	29.0	14
6. $CH_3O + M \rightleftarrows CH_2O + H + M$	13.7	0	21.0	14
7. $CH_2O + M \rightleftarrows HCO + H + M$	16.7	0	72.0	15
8. $CH_2O + H \rightleftarrows HCO + H_2$	13.1	0	3.76	16
9. $CH_2O + O \rightleftarrows HCO + HO$	13.7	0	4.7	17
10. $CH_2O + OH \rightleftarrows HCO + H_2O$	14.7	0	6.3	17
11. $CH_2O + HO_2 \rightleftarrows HCO + H_2O_2$	12.0	0	8.0	18
12. $HCO + M \rightleftarrows CO + H + M$	14.2	0	19.0	19
13. $CH_4 + OH \rightleftarrows CH_3 + H_2O$	3.54	3.08	2.00	20
14. $CH_4 + H \rightleftarrows CH_3 + H_2$	14.86	0	15.01	21
15. $CH_4 + O \rightleftarrows CH_3 + OH$	7.07	2.08	7.63	22
16. $CH_4 + HO_2 \rightleftarrows CH_3 + H_2O_2$	13.3	0	18.0	7
17. $H + O_2 \rightleftarrows OH + O$	14.3	0	16.8	23
18. $O + H_2 \rightleftarrows OH + H$	10.3	1.0	8.9	24
19. $H + H_2O \rightleftarrows OH + H_2$	14.0	0	20.3	24
20. $O + H_2O \rightleftarrows OH + OH$	13.5	0	18.4	24
21. $H + O_2 + M \rightleftarrows HO_2 + M$	15.2	0	-1.0	24
22. $CH_3 + CH_3 \rightleftarrows C_2H_6$	12.9	0	0	25

Table 2. (Continued)

Reaction	log A	n	E	Reference
23. $C_2H_6 + H \rightleftarrows C_2H_5 + H_2$	14.3	0	10.8	26
24. C_2H_5 (+M) $\rightleftarrows C_2H_4 + H$ (+M)	13.58	0	38.0	26
25. $C_2H_4 + OH \rightleftarrows C_2H_3 + H_2O$	14.0	0	3.5	27
26. $C_2H_4 + O \rightleftarrows HCO + CH_3$	12.7	0	1.6	28
27. $C_2H_3 + M \rightleftarrows C_2H_2 + H + M$	14.9	0	31.5	29
28. $C_2H_2 + O \rightleftarrows CH_2 + CO$	13.8	0	4.0	30

Creighton (31) constructed a simplified closed-form mathematical model of the induction period from the following set of reactions:

$$CH_4 + M \rightarrow CH_3 + H + M \quad (1)$$

$$H + O_2 \rightarrow OH + O \quad (17)$$

$$CH_4 + O \rightarrow CH_3 + OH \quad (15)$$

$$CH_4 + OH \rightarrow CH_3 + H_2O \quad (13)$$

$$CH_3 + O_2 \rightarrow CH_3O + O \quad (5)$$

$$CH_3O + M \rightarrow CH_2O + H \quad (6)$$

Although this mechanism is incomplete in its description of methyl-radical oxidation and hydrogen-oxygen combustion, has no formaldehyde decomposition and no C_2 carbon pathways and has only one initiation reaction, it is still useful for prediction of ignition times over a limited range of reaction conditions.

If one assumes that the values of $[CH_4]_o$, $[O_2]_o$, and $[M]_o$ remain constant during the induction period, then the rate equations from the above scheme become a set of linear differential equations. In addition, from previous numerical calculations, it is known that the

$[CH_3O]$, [H], [OH] and [O] radicals are in steady state. With these approximations, the rate equations can be solved for the change in methyl radical concentration to give Equation [2]

$$d[CH_3]/dt = 4k_5[O_2]_o[CH_3] + 4k_1[M]_o[CH_4]_o \ . \qquad [2]$$

Equation [2] is readily integrated to give Equation [3]

$$[CH_3] = \frac{k_1[M]_o[CH_4]_o}{k_5[O_2]_o}[\exp(4k_5[O_2]_o t) - 1] \ , \qquad [3]$$

the time dependence of the methyl radical concentration. The methane concentration dependence is expressed in Equation [4]

$$-d[CH_4]/dt = 5k_5[O_2]_o[CH_3] + 4k_1[M]_o[CH_4]_o \qquad [4]$$

which upon substitution for the methyl-radical concentration yields Equation [5]

$$-d[CH_4]/dt = 5[M]_o[CH_4]_o[\exp(4k_5[O_2]_o t) - 1] + 4k_1[M]_o[CH_4]_o \qquad [5]$$

which can be integrated to give Equation [6],

$$\frac{[CH_4]_o - [CH_4]}{[CH_4]_o} = \left(\frac{5k_1[M]_o}{4k_5[O_2]_o}\right)[\exp(4k_5[O_2]_o t) - 0.8\,k_5[O_2]_o t - 1] \qquad [6]$$

the fraction of methane consumed. When 10% of the methane is consumed, the rate of reaction becomes very large, ending the induction period. Let τ be the ignition time; rearrangement of Equation [6] yields Equation [7]

$$\tau = \left(\frac{1}{4k_5[O_2]_4}\right) \ln\left[\left(\frac{0.08\,k_5[O_2]_o}{k_1[M]_o}\right) + (0.8\,k_5[O_2]_o\,\tau) + 1\right] . \qquad [7]$$

Using initial values for $[O_2]_0$ and $[M]_0$ and the following rate constants:

$$k_1 = [1.95 \times 10^{17} \exp(-88.4/RT)]/[1 + 1.59 \times 10^2 [M]_0 \exp(16/RT)],$$

$$k_5 = 2.51 \times 10^{13} \exp[-29.0/RT],$$

τ may be easily obtained by an iterative solution. Solutions to Equation [7], obtained from a program written for HP-41C calculator, were compared with results from shock-tube-ignition studies performed by Tsuboi and Wagner (5) and Skinner et al. (7) and the calculated results of Creighton (31), in Figures 2 and 3.

The calculated results of Creighton appeared to be in error. In his derivation of the ignition-time formula, the thermal decomposition of methane was incorrectly omitted from his rate expression for methane disappearance. This term was found to make a significant contribution to the rate of reaction. In addition, Creighton did not include the density dependence of the initiation reaction, this omission has an even greater effect on the results. Creighton's result, shown in Figure 2, is far below the experimental results in the high-density study.

The experimental and calculated results in Figure 2 were within the range of experimental error at temperatures 1500 to 2000K. The dependence of the total density on the ignition time obtained from experimental results agreed well with the calculation except at the low-temperature end of the high-density data. The experimentally determined density profile was similar to the one used in the methane-decomposition rate constant.

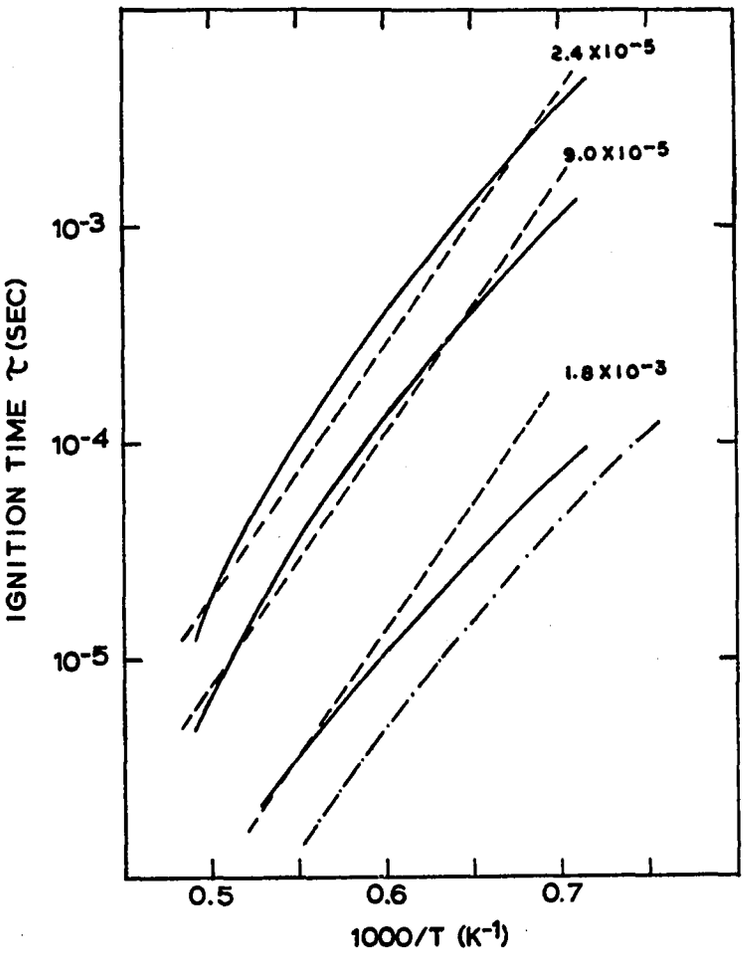

Figure 2. Comparison of ignition times for 0.2% CH_4 and 2.0% O_2 in Ar at various total densities (moles/cm^3):

(———) calculated from Equation [7]
(– – –) experimental result from Reference (5)
(–•–•–) calculated result from Reference (31)

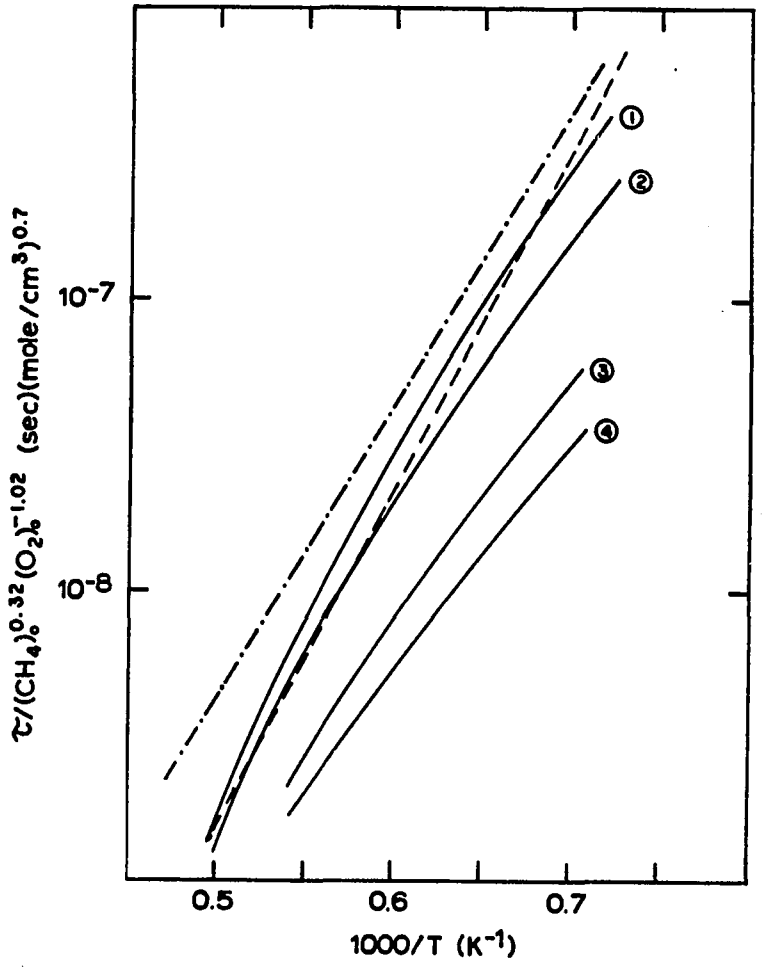

Figure 3. Comparison of reduced ignition times:

(—•—•—) experimental result from Reference (7)
(— — —) experimental result from Reference (5)
(———) calculated result from Equation [7] for various mixtures:

(1) 0.2% CH_4 and 2.0% O_2 in Ar at 2.4×10^{-5} (moles/cm^3)
(2) 0.05% CH_4 and 0.5% O_2 in Ar at 1.5×10^{-3} (moles/cm^3)
(3) 2.0% CH_4 and 2.0% O_2 in Ar at 1.8×10^{-3} (moles/cm^3)
(4) 6.7% CH_4 and 6.7% O_2 in Ar at 8.0×10^{-3} (moles/cm^3)

At higher methane-oxygen concentrations, and in methane-rich reaction mixtures, the calculated ignition times shown in Figure 3 were too short. According to Tsuboi (32), thermal explosions cause local differences in reaction rates and, therefore, inhomogeneity in the reaction mixture. Thus, reliable quantitative information on the reaction mechanism in shock tube experiments can only be obtained if the methane-oxygen mixture is highly diluted with argon (less than 3% methane and oxygen in argon). Since the above mechanism was chosen specifically for a stoichiometric to lean reaction mixture, the low calculated results for ignition times in methane-rich mixtures were not surprising.

In a methane-rich mixture, the hydrogen-atom attack of oxygen, reaction (17) of Creighton's scheme, should be replaced by reaction (14), the hydrogen-atom attack of methane. The resulting set of kinetic equations may then be resolved to give Equation [8]

$$\tau' = \left(\frac{1}{2k_5[O_2]_o}\right) \ln\left[\left(\frac{0.0667\ k_5[O_2]_o}{k_1[M]_o}\right) + (0.667\ k_5[O_2]_o\tau') + 1\right] \qquad [8]$$

where τ' is the ignition time for a fuel-rich mixture. The results of Equation [8] were compared to the results of Equation [7] in Figure 4. The new mechanism yielded an improved prediction of the ignition times, but for the high-density mixtures at lower temperatures and for the mixtures with greater than 3% methane and oxygen in argon, the calculated results were still too low. At low temperatures and high reactant concentrations, reactions (2), (4), (21) and (22) (not

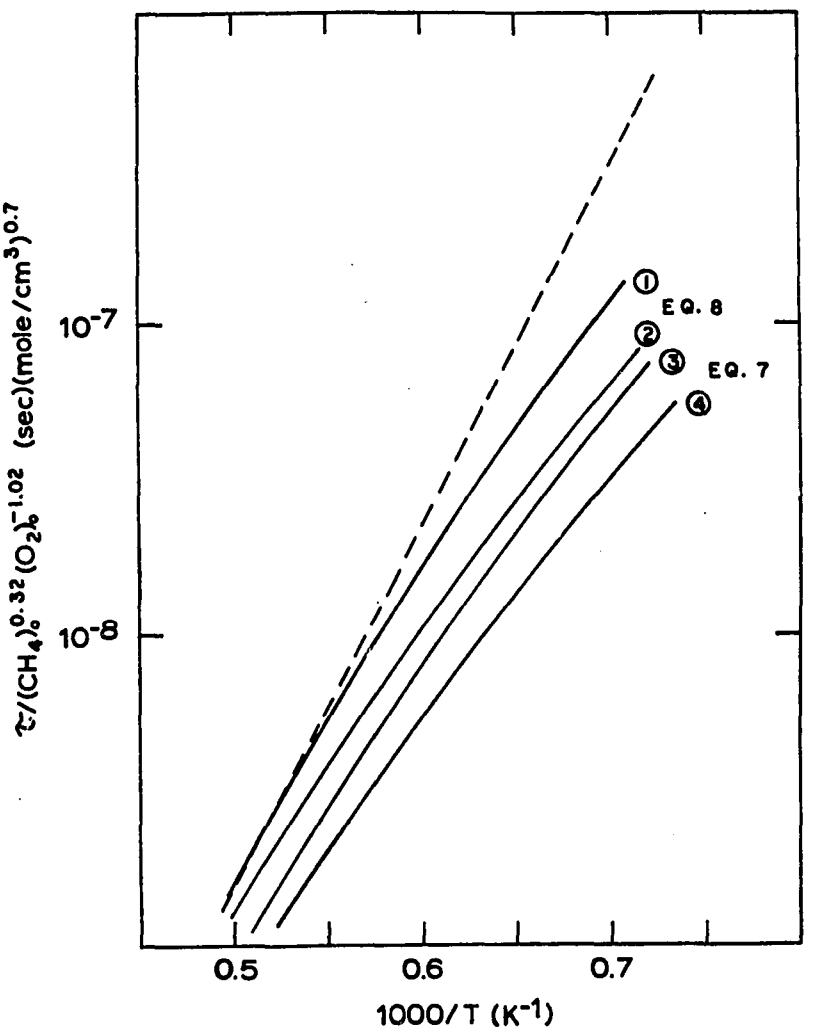

Figure 4. Comparison of reduced ignition times:

(– – –) experimental result from Reference (5)
(———) calculated results from Equations [7] and [8] for various mixtures:

(1) 2.0% CH_4 and 2.0% O_2 in Ar at 1.8×10^{-3} (moles/cm^3)
(2) 6.7% CH_4 and 6.7% O_2 in Ar at 8.0×10^{-3} (moles/cm^3)
(3) 2.0% CH_4 and 2.0% O_2 in Ar at 1.8×10^{-3} (moles/cm^3)
(4) 6.7% CH_4 and 6.7% O_2 in Ar at 8.0×10^{-3} (moles/cm^3)

included in Creighton's scheme) increase in importance; thus, their omission from the above mechanism may be the cause for the poor agreement between calculated and experimental values at these reaction conditions.

The effective activation energy for methane disappearance during the induction period may be determined from the slopes of the curves plotted in Figures 3 and 4. In the 1500 to 2000K temperature range, the slopes correspond to an effective activation energy of 40-60 kcals/mole, which is comparable to the results of Tsuboi and Wagner (5) and Skinner et al. (7), 53.06 and 46.5 kcals/mole, respectively. The literature values for effective activation energies in Table 3, determined by varying analyses of data from shock-tube ignition experiments, range from 20 kcals/mole at low temperature to 100 kcals/mole at high temperature; this effect is not unreasonable from the present results.

In the main reaction period, methane and the intermediate species are oxidized to the final products, water, carbon dioxide and thermal energy. Reactions in the main reaction period are much faster than either the initiation or chain-branching phase reactions of the induction period. During the methane-consumption phase, methane is converted into carbon monoxide, water and 68% of the overall heat of reaction is produced. The carbon monoxide-oxidation phase produces carbon dioxide and the remaining 32% of the thermal energy.

The reactions which are important at the end of the induction period remain important during the methane-consumption phase; but as

Table 3. Results from shock-tube ignition-time experiments

Effective Activation Energy (kcals/mole)	Temperature Range (K)	Reference
20.6	900 to 1350	33
21.5	1050 to 2100	34
25.3 to 30.6	740 to 855	35
32.0	1800 to 2500	36
33.0	1150 to 2500	37
33.0	1250 to 2500	38
33.8	1250 to 2500	34
38.1 to 63.4	1200 to 1800	39
42.0	1850 to 2200	40
46.5	1500 to 2150	7
49.5	1420 to 2010	41
51.0	1200 to 2000	42
51.4	1350 to 1900	43
52.9	1350 to 1850	33
53.1	1200 to 2100	5
56.0	2000 to 2300	9
62.0	1700 to 2500	40
65.0	1450 to 2100	44
80.0, 100.0	2100 to 2500	8

radical concentrations increase additional reactions begin to occur. The overall stoichiometry of the methane-consumption phase is given by $CH_4 + \frac{3}{2} O_2 \rightleftarrows CO + 2H_2O$. Twice as much water as carbon monoxide is produced during this phase. Reaction (13)

$$CH_4 + OH \rightleftarrows CH_3 + H_2O \qquad (13)$$

is responsible for most of the water production, since this reaction occurs at the molecular collision frequency. The reverse of Reactions (1) and (2)

$$CH_3 + H + M \rightleftarrows CH_4 + M \qquad (-1)$$

$$CH_3 + HO_2 \rightleftarrows CH_4 + O_2 \qquad (-2)$$

balance rates of creation and consumption of the hydrogen atoms and hydroperoxyl radicals, and also recycle a significant portion of the methyl radicals to methane. Oxygen atoms react with water through Reaction (21)

$$O + H_2O \rightleftarrows OH + OH \qquad (20)$$

yielding two hydroxyl radicals. Hydrogen, C_2 carbon species, and formaldehyde are all rapidly oxidized during the methane consumption phase.

The carbon monoxide-oxidation phase is delayed until nearly all the C-H and H-H bonds have been broken. Most of the carbon monoxide is consumed by reaction with hydroxyl radicals through Reaction (29)

$$CO + OH \rightleftarrows CO_2 + H \; . \qquad (29)$$

The rate of consumption of carbon monoxide will be directly related to the availability of hydroxyl radicals. Reactions of hydroxyl radicals with hydrocarbons keep this radical's concentration at low levels. Thus, once all the hydrocarbons have reacted, the hydroxyl-radical concentration increases and Reaction (29) increases in rate. Dryer et al. (45) has shown that Reaction (29) has a very strong non-classical temperature dependence; this reaction under typical reaction conditions, is favored over the spin-forbidden, chemiluminescent reaction of oxygen atoms with carbon monoxide, Reaction (30)

$$CO + O + M \rightleftarrows + CO_2 + M \ . \qquad (30)$$

The reactions of hydrogen and oxygen atoms and hydroperoxyl radicals with the C-H bonds of methane and intermediate species, and with hydrogen molecules occur at rates which are greater than or comparable to that of reaction (29); thus, these radical species' concentrations also remain low until nearly all the C-H and H-H bonds have been broken.

The carbon monoxide-oxidation phase, above 2000K, is dominated by the following four reactions

$$CO + OH \rightleftarrows CO_2 + H \qquad (29)$$

$$H + O_2 \rightleftarrows OH + O \qquad (17)$$

$$O + H_2O \rightleftarrows OH + OH \qquad (20)$$

$$H + OH + M \rightleftarrows H_2O + M \ . \qquad (31)$$

Reaction (17) is an important reaction in both the induction and the main reaction periods. Branching in Reactions (17) and (20) increases radical concentrations until the destruction of radicals by Reaction (31)

becomes important. It has been found by Dryer and Glassman (46) that the hydroxyl-radical concentration exceeds the equilibrium value of Reaction (31) by two orders of magnitude; thus, this reaction must not become important until the latter stages of the carbon monoxide-oxidation phase.

At temperatures around 1000K, a slightly different set of reactions dominates the carbon monoxide-oxidation phase. At lower temperatures, Reaction (31) is replaced by Reaction (21)

$$H + O_2 + M \rightleftarrows HO_2 + M \qquad (21)$$

as a consumer of hydrogen atoms (at temperatures above 2000K, Reaction (31) dominates because Reaction (21) approaches equilibrium). Rate-constant parameters for Reactions (29), (30) and (31) are given in Table 4. Carbon monoxide oxidation is relevant to the combustion of

Table 4. Main-reaction-period rate constants for forward reactions $k = AT^n\exp(-E/RT)$ in cm^3, mole, sec, kcal, K units

	Reaction	log A	n	E	Reference
29	$CO + OH \rightleftarrows CO_2 + H$	7.1	1.3	-0.8	47
30	$CO + O + M \rightleftarrows CO_2 + M$	15.8	0	4.1	48
31	$H + OH + M \rightleftarrows H_2O + M$	23.88	-2.6	0	49

methane under most experimental reaction conditions immediately following the oxidation of hydrocarbon to carbon monoxide.

The oxidation of hydrogen and carbon monoxide has been exhaustively studied. High levels of information on the elementary reactions has been presented. For all experimental and practical regions of interest, major reaction pathways are understood and the corresponding rate-constant expressions are known (10).

The preceding material summarized the reactions believed to occur by the majority of kineticists in the methane-oxygen system. Numerous variations for methane-oxygen combustion mechanisms have been suggested in the literature; recent reviews include Olson and Gardiner (13), Tsuboi (32), Bowman (17) and Westbrook et al. (19). The main differences between these mechanisms were found in methyl-radical oxidation, formaldehyde decomposition and C_2 carbon pathways.

Some Aspects of Methyl Radical Formation and Consumption

The rates of elementary reactions between initial components are important because they are responsible for the production of original active centers such as simple atoms, free radicals and reactive intermediates. These reactions are usually highly endothermic, contribute only a small fraction of the overall active centers and are quite slow. Yet, the overall mechanism is directly sensitive to changes in the rate constants of reactions involving methane, oxygen and argon since the concentrations of these initial components are quite high and only vary slowly during the induction period.

The initiation phase of methane-oxygen combustion is marked by the appearance and increase in concentration over several orders of magnitude of methyl radicals. Several theoretical and experimental results have been employed by various workers in an attempt to characterize the nature of the initial methyl-radical production in methane oxidation.

In the temperature region above 1700K, the primary-thermal-decomposition reaction of methane is fairly well established as:

$$CH_4 + M \rightleftarrows CH_3 + H + M \qquad (1)$$

followed by hydrogen-atom abstraction

$$CH_4 + H \rightleftarrows CH_3 + H_2 \qquad (14)$$

The rate of reaction (1) reported by Hartig et al. (11), Roth and Just (21), Heffington et al. (8) and Tabayashi and Baur (50) was found to be in fairly good agreement over the temperature range 1700 to 2800K. At 2000K, the rate constants differ by less than 50% with an average value of 3.8×10^7 cm^3/mole·sec, see Table 5.

Table 5. Reaction (1) $CH_4 + M \rightarrow CH_3 + H + M$ rate-constant data
$k = A \exp(-E/RT)$ in cm^3, mole, sec, K, kcal units

Reference	log A	E	Experimental Details
12	17.30	88.0	ir emission of CH_4 behind reflected shock waves, 0.2 to 1.0% CH_4, in Ar 5.5×10^{-5} to 1.5×10^{-3} moles/cm^3, 1850 to 2500 K
12[a]	15.1	104.0	

[a]High-density first-order rate constant.

Table 5. (Continued)

Reference	log A	E	Experimental Details
46	17.67	93.2	H-atom absorption behind reflected shock waves, 5 to 200 ppm CH_4 in Ar, 1.5×10^{-5} moles/cm^3, 1700 to 2300K
44	17.34	90.1	emission and absorption of CH_4 behind reflected shock waves, 2 to 5% CH_4 in Ar, 1.0×10^{-5} to 2.5×10^{-5} moles/cm^3, 2023 to 2721K
50	17.00	85.8	post incident shock density-gradient, 10 to 20% CH_4 in Ar, 2.37×10^{-6} to 8.9×10^{-3} moles/cm^3, 1950 to 2770K

At lower temperatures, the direct decomposition of methane is too slow, and the initiation step probably involves methane and oxygen via Reaction (2)

$$CH_4 + O_2 \rightleftarrows CH_3 + HO_2 \qquad (2)$$

followed by hydroperoxyl radical attack of methane

$$CH_4 + HO_2 \rightleftarrows CH_3 + H_2O_2 \qquad (16)$$

This mode of initiation was first suggested for higher paraffins by Cullis and Hinshelwood (51) and later was substantiated theoretically by Semenov (52). Although an experimental measurement of Reaction (2) has not been reported, the theoretical estimates of Skinner et al. (7),

Fristrom and Westenberg (53), and Denisov (54) for this rate have been widely used, see Table 6.

Table 6. Reaction (2) $CH_4 + O_2 \rightleftarrows CH_3 + HO_2$ rate-constant data
$k = A \exp(-E/RT)$ in cm^3, mole, sec, K, kcal units

Reference	log A	E	Details of Estimate
11	13.9	56.0	A value estimated a little larger than the A value for $H_2 + O_2$ initiation, activation energy slightly greater than enthalpy of reaction
53	14.0	55.0	A value from maximum collision theory frequency, activation energy from minimum heat of reaction
54	12.6	55.0	A value from activated complex partition functions, activation energy from minimum heat of reaction

The values of Skinner et al. and Fristrom and Westenberg are in agreement. The pre-exponential factor of Denisov is less than the collision frequency estimate of Fristrom and Westenberg by more than a factor of 10. This discrepancy is most likely due to an error in Denisov's calculation of the activated-complex rotational partition function, combined with the omission of the statistical factor from Fristrom and Westenberg's pre-exponential value.

Taking Fristrom and Westenberg's theoretical estimate as the upper limit of the rate constant for Reaction (2) and the density-dependent value of the Reaction (1) rate constant from the pyrolysis studies of Hartig et al. (11), the following ratio, given by Equation [9],

$$R = k_2[O_2]/k_1[M] = [10^{3.3}\exp(33/RT)][1 + [M]10^{2.2}\exp(16/RT)] + [M]10^{2.2}\exp(16/RT)]([O_2]/[M]) \quad [9]$$

may be obtained. R, as a function of reciprocal temperature, was plotted by Heffington et al. (8) for various ratios of oxygen to argon at a total density of 6×10^{-6} moles/cm^3. A 10% precision in rate estimates requires that both initiation reactions be included in kinetic studies from 1300 to 2200K, see Figure 5. At 1400K, Reaction (2) has a rate-constant value of 2.6×10^5 cm^3/mole sec.

The rate of initiation affects the overall length of the induction period. The thermal decomposition of methane is widely accepted as the mode of initiation at elevated temperatures. The importance and even existence of hydrogen abstraction by oxygen from methane has been questioned by some authors (50) and accepted by others (54).

The rate constants for methane reactions with hydrogen and oxygen atoms and hydroxyl radicals have been fairly well established.

Zellner and Steinert (20) used a flash-photolysis system to study Reaction (13)

$$CH_4 + OH \rightleftarrows CH_3 + H_2O \quad (13)$$

from 300 to 900K by monitoring OH absorption. More recently, Ernst et al. (55) confirmed the previously suggested non-Arrhenius behavior

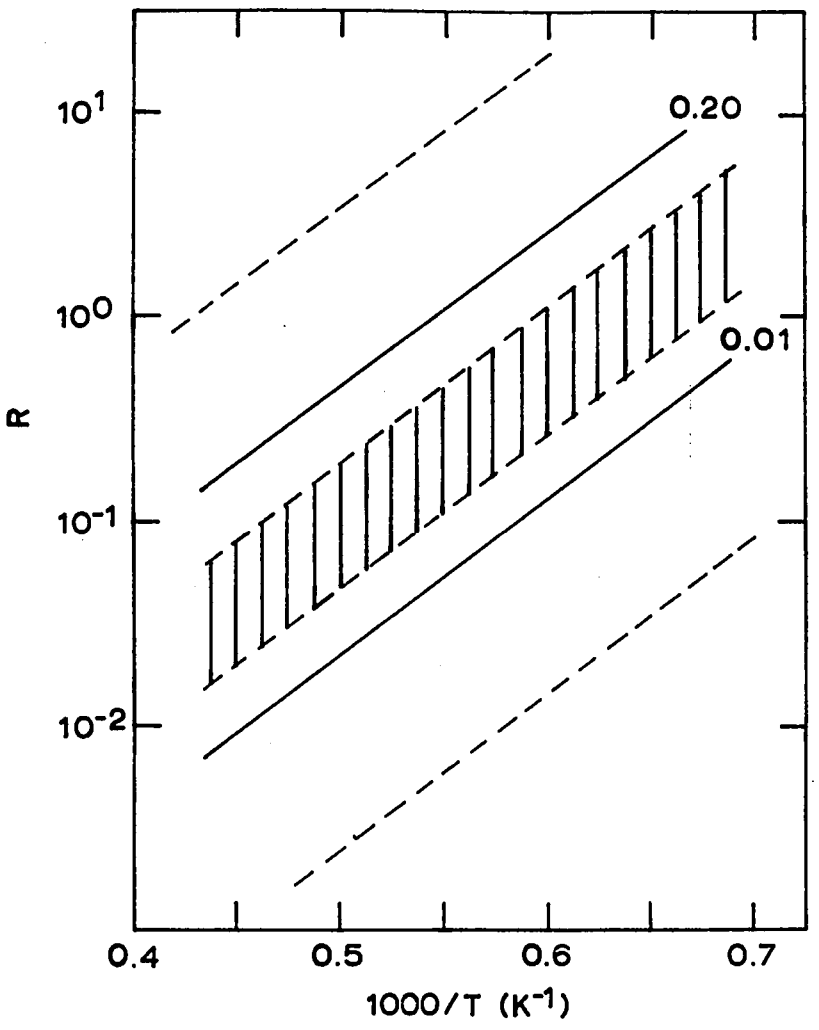

Figure 5. Values for the ratio R from Equation [9] (———), for various $(O_2)/(M)$ ratios, $M = 6 \times 10^{-6}$ (moles/cm^3). Shaded area indicates the overlap in the uncertainty in R. From Reference (44)

of this reaction in a combined flash-photolysis, shock-tube experiment. Roth and Just (21) have measured the rate of Reaction (14)

$$CH_4 + H \rightleftarrows CH_3 + H_2 \qquad (14)$$

in a shock tube from 1700 to 2300K. Peeters and Mahnen (56) have studied this reaction at 1600K in methane-oxygen flames. Reaction (15)

$$CH_4 + O \rightleftarrows CH_3 + OH \qquad (15)$$

was studied by Roth and Just (22) by following the oxygen-atom concentration in the reaction zone behind reflected shock waves in methane-nitrous oxide mixtures from 1500 to 2250 K. Curved Arrhenius behavior has been found and well characterized for each of the above methane-radical reactions.

The number of possible reactions which follow the methane chain initiation sequence is very great. Of concern here is the fate of the methyl radicals. The two most important methyl-radical reactions are its reaction with oxygen atoms and with other methyl radicals.

The mechanism and rate of the $CH_3 + O_2$ reaction continues to be a matter of concern. Reitel'boim *et al.* (57) performed a calculation based on RRKM theory (58) and proposed that the interaction of methyl radicals with oxygen proceeds along three channels: an addition channel, Reaction (32)

$$CH_3 + O_2 \ (+M) \rightleftarrows CH_3O_2 \ (+M) \ , \qquad (32)$$

and two direct channels, Reactions (5) and (4)

$$CH_3 + O_2 \rightleftarrows CH_3O + O \quad (5)$$

$$CH_3 + O_2 \rightleftarrows CH_2O + OH \quad (4)$$

According to Reitel'boim et al. the existence of an addition reaction channel necessitates the formation of a long-lived methylperoxy complex. Basco et al. (59) have studied the kinetics of methylperoxy radical formation at 295K from 25 to 380 torr. The order of reaction (32) was between 3 and 2 throughout the range of the experimental conditions. The limiting value of the third-order low-pressure rate coefficient was found to be 9.4×10^{16} $cm^6/mole^2 \cdot sec$. The limiting value of the second-order high-pressure rate coefficient was found to be 3.1×10^{11} $cm^3/mole \cdot sec$.

Reaction (5) has been studied by Brabbs and Brokaw (14) by monitoring the growth of CO flame-band emission behind incident shocks. Methane, carbon monoxide, oxygen and argon mixtures reacted from 1200 to 1800K yielded a rate constant of $2.4 \times 10^{13} \exp(-28.8/RT)$ $cm^3/mole \cdot sec$. Bhaskaran et al. (60) studied Reaction (5) in a shock tube from 1700 to 2300K and found a rate constant of $5 \times 10^{13} \exp(-34.6/RT)$ $cm^3/mole \cdot sec$.

Reaction (4) is generally held to be necessary for describing formaldehyde formation in methane combustion at temperatures below 2000K. A direct determination of the rate constant for Reaction (4) has not been reported. During the past several years, Basco et al. (59), Washida and Bayes (61), Baldwin and Golden (62) and Klais et al. (63) have sought to demonstrate experimentally the existence of this reaction. Unfortunately, the results of these experiments are

inconclusive. The shock-tube work of Izod et al. (64), Clark et al. (65), Bowman (17), Jachimowski (66), Tsuboi (32), Olson and Gardiner (13), Tabayashi and Bauer (50) and Bhasharan et al. (60) provided indirect evidence for the rate of Reaction (4). In each of these determinations, the rate of Reaction (4) was inferred by comparison of observed and calculated experimental results for a chosen overall reaction mechanism.

Reported Reaction (4) rate-constant values are shown in Figure 6. The high-temperature results are close together with activation energies ranging from 9 to 14 kcals/mole. The lone exception is the activation energy of 25.5 kcals/mole reported by Bhaskaran et al. (60). Baldwin and Golden (62) found no evidence for Reaction (4) at 1220K, stating an upper limit for its rate of 3×10^8 cm^3/moles·sec. The results of Baldwin and Golden support the activation energy determined by Bhaskaran et al., and the only measurement which remains in strong disagreement is the low-temperature work of Washida and Bayes (61). Computer analysis of methane combustion performed by various authors (13, 17, 19 and 32) included either Reaction (4) or Reaction (5) in their mechanisms; yet, it is interesting to note that at 2000K, the rate constants for Reactions (4) and (5) determined by Bhaskaran et al. are nearly equal.

The reaction of methyl radicals with other methyl radicals has been intensively studied. For combustion conditions, Reaction (22) is in the pressure-sensitive region, and thus the density dependence for the rate constant must be considered. At a total density of 1.5×10^{-6} moles/cm^3,

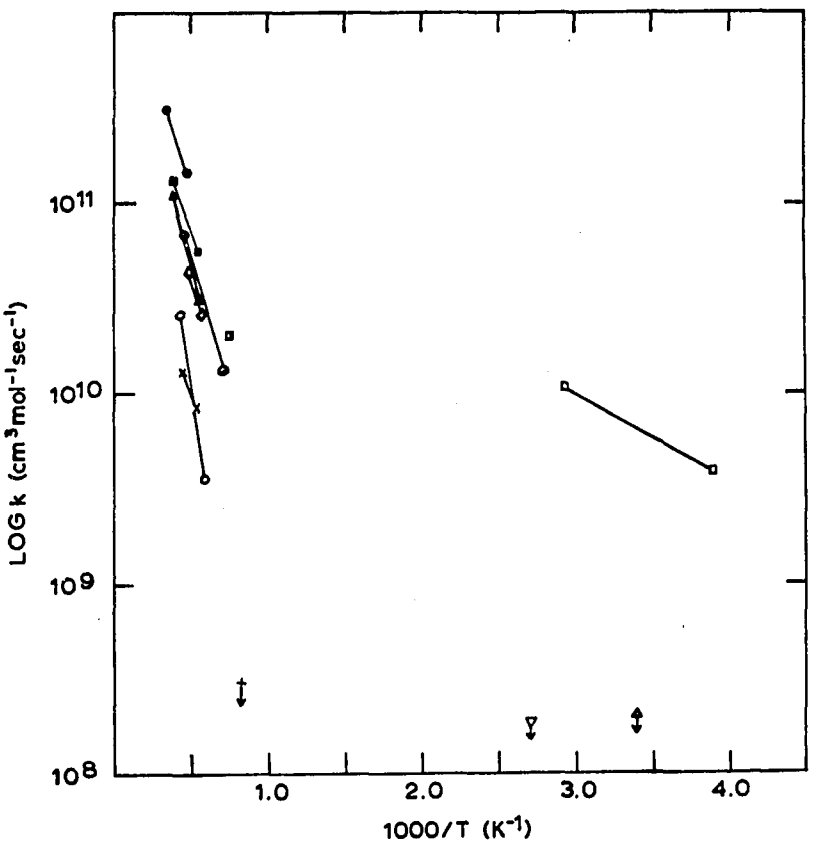

Figure 6. Arrhenius plot of Reaction (4) data. The data sources are: ◐ Reference (64), ◨ Reference (65) upper limit, X Reference (17), ▲ Reference (66), □ Reference (61), △ Reference (59) upper limit, ■ Reference (13), + Reference (62) upper limit, ▽ Reference (62) upper limit, ◇ Reference (32), ● Reference (50), ○ Reference (60)

Clark et al. (25) found a temperature-independent rate coefficient for Reaction (22) of 8.43×10^{12} cm^3/mole·sec, in the temperature range 1120 to 1400K. Clark et al. found that the rate of Reaction (22) increased with pressure. Zaslonko and Smirnov (67) supported the results of Clark et al. and found the high-pressure limit for the rate coefficient to be 1.3×10^{13} cm^3/mole·sec. Zaslanlso and Smirnov also found a decrease in the rate of recombination with an increase in temperature; they reported a temperature-dependent rate in the high-pressure limit of $k_{22}^{\infty} = 1.81 \times 10^{13} (T/1000)^{-0.38}$ cm^3/mole·sec, for the temperature range 300 to 1750K.

The above reactions of methyl radicals occur during the induction period of methane combustion when little heat is produced and active centers such as O, H, HO_2 and OH are at steady-state concentration levels. As the induction period progresses, the methyl-radical concentration increases and the radical concentrations begin to rise in proportion. When methane consumption becomes large enough, the main reaction period begins and the combustion process dramatically increases in rate and heat production.

The rate of the $CH_3 + O_2$ reaction is one of critical importance in determining the length of the induction period. Thus far, the experimental characterization of $CH_3 + O_2$ reaction has been limited to indirect inferences, single-temperature upper-limits and conflicting and inconclusive results.

The Use of Iodine to Produce and Trap Methyl Radicals

The methane-iodine reaction is the most endothermic of all paraffin-halogen reactions. The reactivity of alkanes with halogens varies tremendously as one goes from fluorine to iodine (68). In spite of the vast differences in external appearance, it is a commonly held view that the reactions of all halogens with paraffins may be considered within the framework of the following generalized chain mechanism:

$$X_2 \xrightarrow[\text{agent}]{\text{initiating}} X \qquad (33)$$

$$X + RH \rightleftharpoons R + XH \qquad (34)$$

$$R + X_2 \rightleftharpoons RX + X \qquad (35)$$

$$2R \longrightarrow \qquad (36)$$

$$R + X \longrightarrow \quad \text{nonradical products} \qquad (37)$$

$$2X \xrightarrow{M} \qquad (38)$$

The initiation step generates halogen atoms via Reaction (33). The chain is propagated by Reactions (34) and (35). The attack of a halogen atom on a C-H bond produces alkyl radical and hydrogen halide, Reaction (33); and the attack by an alkyl radical on molecular halogen produces alkyl halide and halogen atom via Reaction (35). The chain is terminated by radical-radical coupling, Reactions (36), (37) and (38). The reverse of Reactions (34) and (35), reactions between alkyl radical

and hydrogen halide and alkyl halide and halogen atom, respectively, play an important role in the iodination of methane.

Flowers and Benson (69) studied the kinetics of the reaction of methyl iodide with hydrogen iodide from 533 to 589K and reported rate constant values for Reactions (40), (-40), (41) and (-41)

$$I_2 + M \rightarrow I + I + M \quad (39)$$

$$CH_4 + I \rightleftarrows CH_3 + HI \quad (40)$$

$$CH_3 + I_2 \rightleftarrows CH_3I + I \quad (41)$$

$$CH_3 + CH_3\ (+M) \rightarrow C_2H_6\ (+M) \quad (22)$$

$$CH_3 + I + M \rightarrow CH_3I + M \quad (42)$$

$$I + I + M \rightarrow I_2 + M \quad (43)$$

Goy and Pritchard (70) studied the kinetics and thermodynamics of the reaction between iodine and methane from 548 to 618K, and determined the rate constant for Reaction (40) and the equilibrium constant for the formation of methyl iodide and hydrogen iodide. The value of the rate constant for Reaction (22) was discussed previously. Saito et al. (71) studied the thermal decomposition of methyl iodide in a shock tube from 1050 to 1500K. The rate of Reaction (-42) was reported, and the temperature dependence of the free-energy of formation of a methyl radical and an iodine atom from methyl iodide was given. The rate of Reaction (-42) was found to be second order and proportional to the total density in the range 3.5×10^{-6} to 3.9×10^{-5} moles/cm^3.

Rate-constant values for the methane-iodine reaction are given in Table 7.

Table 7. Methane-iodine reaction rate constants
$k = A \exp(-E/RT)$ in cm^3, mole, sec, kcal units

Reaction		log A	E	Reference
40	$CH_4 + I \rightarrow CH_3 + HI$	14.70	33.5	69
		14.95	35.04	70
-40	$CH_3 + HI \rightarrow CH_4 + I$	12.40	1.2	69
41	$CH_3 + I_2 \rightarrow CH_3I + I$	12.90	0.4	69
-41	$CH_3I + I \rightarrow CH_3 + I_2$	14.40	20.0	69
22	$CH_3 + CH_3$ (+M) $\rightarrow C_2H_6$ (+M)	12.9	0	25
42	$CH_3 + I + M \rightarrow CH_3I + M$	See text	See text	71

The kinetics of iodine dissociation, Reaction (39), was studied in a shock tube from 1060 to 1860K by Britton et al. (72). Blake and Burns (73) studied the kinetics of iodine-atom recombination, Reaction (43), by flash photolysis from 300 to 1164K. The rate constant for Reaction (43) calculated from shock-tube dissociation rate data was significantly higher and had a greater temperature dependence than the rate determined directly from the flash-photolysis recombination rate experiments. Although there was a significant difference in rates, the forward and reverse rate constants reported by Britton et al. (72) were used for Reactions (39) and (43), respectively, since these results were obtained from the shock-wave dissociation of iodine.

It was decided that an extension of the rate constant data of Goy and Pritchard (70) for Reaction (40) to higher temperatures could be measured in a single-pulse shock tube, by reacting mixtures of argon, methane and iodine tagged with radioactive iodine-131. This proposed study of Reaction (40) would require the use of radiochemical methods to obtain a quantitative determination of methyl iodide production.

It was proposed that the rate of production of methyl radicals resulting from the methane-oxygen initiation, Reaction (2), could be subsequently studied upon addition of small amounts of oxygen to the argon-methane-radio iodine mixture. The resulting methyl-radical production from Reaction (2) would be detected as an increase in methyl iodide formation, since iodine would serve to trap the additional methyl radicals via Reaction (41).

The most important uses of kinetic data on elementary reactions at high temperatures are in modeling of combustion systems and in providing information on the pressure dependence of unimolecular and the non-Arrhenius behavior of bimolecular reactions.

Direct kinetic investigations of combustion reactions are of notorious difficulty for two good reasons. Firstly, elementary processes are difficult to isolate kinetically due to the complex composition of combustion mixtures. Secondly, at elevated temperatures, sensitivity for various active centers decreases greatly due to these species' short lifetimes and high reactivities.

In view of these problems, it is not surprising that an experimental determination of the methane-oxygen initiation reaction has yet

to be reported. Thus, it was decided to attempt a study of Reaction (2) in a single-pulse shock tube employing the above mentioned radiochemical techniques. The rapid and efficient removal of methyl radicals by iodine would establish a steady-state concentration of methyl radicals and thus eliminate additional methane-combustion chain reactions. The overall sensitivity of the technique is limited mainly by the extent of methyl iodide formation via the methane-iodine halogenation process.

THE SHOCK TUBE METHOD AND THEORY

The general features of the single-pulse-shock-tube technique and the ideal one-dimensional shock-tube theory have been adequately described by Kassman (74). The purpose of this chapter is to provide a brief summary of the shock-tube method and a description of the ideal shock-tube theory employed in calculation of the reaction mixture gas dynamic state.

Shock Tube Method

A shock wave results when an object passes through a medium at a velocity which is greater than the speed of sound in that medium. Hence, the medium in front of the object is totally unprepared for the arrival of the object. The increase in pressure, temperature, and density of the shocked medium results in the propagation of a shock-wave discontinuity through the medium.

The use of shock waves for chemical studies of gas-phase reaction rates was made possible by the development of the shock tube. In the single-pulse shock tube, the experimenter can react a gas sample of desired composition in a single heating and cooling cycle of known amplitude and duration. Spectroscopic analysis of the reaction mixture behind the reflected shock wave during the course of the reaction and/or chemical analysis of the quenched reaction products after the passage of the cooling wave through the reaction gas mixture allows the kineticist to study fast reactions at high temperatures for short reaction times.

Symbolism

Listed below is the set of symbols used in the text:

1)	a (cm/sec)	Speed of sound
2)	c_p (erg/g·K)	Specific heat
3)	C_p° (erg/mole·K)	Molar heat capacity
4)	h (erg/g)	Specific enthalpy
5)	H° (erg/mole)	Standard state enthalpy
6)	K_T (atm)	Equilibrium constant
7)	M (g/mole)	Molecular weight
8)	P (dyn/cm^2)	Pressure
9)	P_{fi}	Ratio of gas pressure across stock wave, f to i
10)	R (erg/mole·K)	Perfect gas constant
11)	T (K)	Temperature
12)	T_{fi}	Ratio of gas temperature across shock wave, f to i
13)	u (cm/sec)	Velocity of gas with respect to the shock tube
14)	v (cm/sec)	Velocity of gas with respect to the shock wave
15)	X°	Initial mole fraction
16)	γ	Ratio of heat capacities, c_p to c_v
17)	ρ (g/cm^3)	Density
18)	ρ_{fi}	Ratio of gas density across shock wave, f to i
19)	ϕ	Fraction of dissociation

Ideal Shock Tube Theory

Ideal one-dimensional shock-tube theory is derived from a combined application of thermodynamics and Newtonian Mechanics. The experimental conditions of high temperature, low density and pressure and high dilution of reactants in argon found in conventional shock tubes allows one to make use of the following set of assumptions: 1) the effects due to heat conduction and viscosity are small. 2) The heat of reaction behind the reflected shock wave is negligible. 3) The reactant gas obeys the ideal gas law.

The speed of sound in a gas is given by Equation [10]. The

$$a = [\gamma P/\rho]^{1/2} \qquad [10]$$

conservation of mass, energy and momentum across a shock wave, are given in Equations [11], [12] and [13], respectively,

$$\rho_i v_i = \rho_f v_f \qquad [11]$$

$$h_i + \frac{1}{2} v_i^2 = h_f + \frac{1}{2} v_f^2 \qquad [12]$$

$$P_i + \rho_i v_i^2 = P_f + \rho_f v_f^2 \ . \qquad [13]$$

The enthalpy change in a shocked gas is given by Equation [14]

$$h = c_p T \ (+ \text{constant}) \ , \qquad [14]$$

where c_p is a known function of temperature. The equation of state for an ideal gas is given by Equation [15]

$$PM = \rho RT \ . \qquad [15]$$

From Equations [10] through [15], the measurement of the incident shock velocity and a knowledge of the initial reaction gas conditions, the thermodynamic state of the gas behind the reflected shock wave may be calculated.

The gas velocities found in Equations [11], [12] and [13] were determined relative to the shock wave. With the shock wave at the origin of the coordinate system, all gas velocities were positive, see Figure 7. The variables' subscripts refer to the region of gas, where i denotes the initial gas in front of the shock wave and f denotes the final gas behind the shock wave. Numbered subscripts refer to the regions of gas consistent with Figure 8.

Before an application of Equations [10] through [15] to the four-component system (argon, methane, oxygen and iodine) is made, it is worthwhile to gain some familiarity with manipulation of the shock-tube equations by studying the simplified argon case. In this derivation, argon is the single component in the shocked gas, no chemical reaction occurs and the following two relationships hold:

$$M_i = M_f \qquad [16]$$

$$c_p = \frac{5}{2} R/M \qquad [17]$$

The initial and final molecular weights are equal in both the incident and reflected shock cases, and the specific heat is independent of temperature.

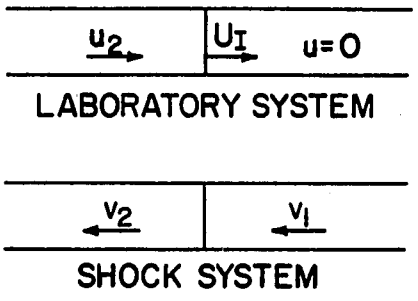

Figure 7a. Incident shock-wave coordinate systems

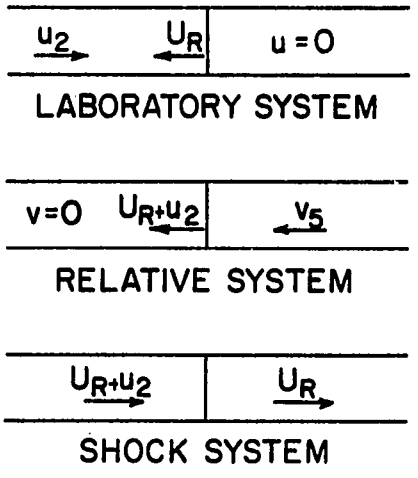

Figure 7b. Reflected shock-wave coordinate systems

Figure 7. Coordinate systems for gas flow in the shock tube. From Reference (74, p. 29)

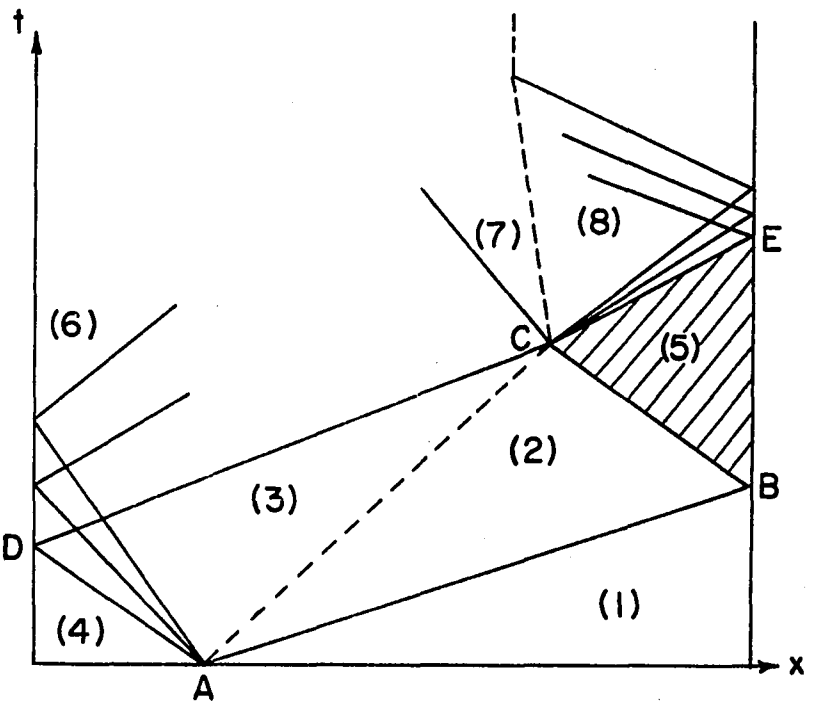

Figure 8. Phenomena in the single-pulse shock tube illustrated in x-t coordinates. From Reference (74, p. 12)

Prior to experiment: diaphragm at point A separates initial gases, high-pressure driver gas (4) and low-pressure reactant gas (1).

After diaphragm is ruptured: incident shock wave, line AB, passes through gas (1), and gas (2) behind incident shock wave is formed. The contact surface, line AC, separates compressed reactant gas (2) and expanded driver gas (3). Expansion waves, lines AD and DC, pass through initial driver gas (4) and expanded driver gas (3). Reflected shock wave, line BC, passes through gas (2) and gas (5) behind reflected shock wave is formed. Expansion wave, contact surface and reflected shock wave interact at point C to generate a cooling wave, line CE, which quenches the reaction mixture, gas (5).

Rearrangement of Equation [13] yields Equation [18]

$$P_i - P_f = \rho_f v_f^2 - \rho_i v_i^2 \qquad [18]$$

and rearrangement of Equation [11] yields Equation [19]

$$v_f = (\rho_i/\rho_f)v_i \ . \qquad [19]$$

The square of v_f from Equation [19] may be substituted into Equation [18] to give Equation [20]

$$P_i - P_f = \rho_i \ v_i^2(\rho_{fi} - 1) \ . \qquad [20]$$

Both sides of Equation [20] may be divided by P_i; ρ_{fi} may be replaced by P_{fi}/T_{fi} (derived from Equations [15] and [16]) to yield Equation [21]

$$1 - P_{fi} = v_i^2(\rho_i/P_i)((T_{fi}/P_{fi}) - 1) \ . \qquad [21]$$

Rearrangement of Equation [21] yields Equation [22]

$$v_i = [(P_i/\rho_i)(P_{fi} - 1)/(1 - (T_{fi}/P_{fi}))]^{1/2} \ , \qquad [22]$$

the initial shock frame gas velocity.

In the incident-shock-wave case $i = 1$ and $f = 2$, v_i is measured from the incident shock velocity and P_i, ρ_i, and T_i are determined from the initial conditions. There remain two unknowns in Equation [22], namely P_f and T_f; thus, a second independent relationship must be derived.

Rearrangement of Equation [13] yields Equations [23a] and [23b]

$$(P_i - P_f)(1/\rho_i) = (\rho_f/\rho_i)v_f^2 - v_i^2 \qquad [23a]$$

$$(P_i - P_f)(1/\rho_f) = v_f^2 - (\rho_i/\rho_f)v_i^2 \ , \qquad [23b]$$

which may be added to give Equation [24]

$$(P_i - P_f)(1/\rho_f + 1/\rho_i) = v_f^2 - v_i^2 \ . \qquad [24]$$

Rearrangement of Equation [12] yields Equation [25]

$$h_f - h_i = \frac{1}{2}(v_i^2 - v_f^2) \ , \qquad [25]$$

which upon substitution into Equation [24] yields Equation [26]

$$(P_i - P_f)(1/\rho_f + 1/\rho_i) = 2(h_i - h_f) \ . \qquad [26]$$

From Equations [14] and [17], Equation [27]

$$2(h_i - h_f) = (5R/M)(T_i - T_f) \qquad [27]$$

is derived. Substitution of $h_i - h_f$ from Equation [27] into [26] yields Equation [28]

$$(P_i - P_f)(1/\rho_f + 1/\rho_i) = (5\ R/M)(T_i - T_f) \qquad [28]$$

Equation [28] may be converted into Equation [29]

$$P_{fi}^2 + P_{fi}\ (4 - 4\ T_{fi}) - T_{fi} = 0 \qquad [29]$$

by algebraic rearrangement and the use of Equations [15] and [16]. Equation [29] is a second order polynomial in P_{fi}. The appropriate root in Equation [29] is given by Equation [30]

$$P_{fi} = 2(T_{fi} - 1) + [4(T_{fi} - 1)^2 + T_{fi}]^{1/2} \ . \qquad [30]$$

Again, in the incident-shock-wave case $i = 1$ and $f = 2$, thus the only unknowns in Equation [30] are P_f and T_f. Equations [22] and [30] are a pair of independent equations with two unknowns; it is readily seen that from these two equations the final state of the gas behind the

the incident shock wave may be uniquely determined by an iterative solution.

In the reflected-shock-wave case, the same equations apply, only here $i = 2$ and $f = 5$. In the reflected case, the initial gas velocity, v_i, of Equation [22], cannot be measured directly, thus, it must be calculated from the region 2 state variables. The region 2 lab-frame gas velocity, u_2, expressed in Equation [31] is very useful here. It

$$u_2 = v_i - v_f = v_1 - v_2 = v_2^* - v_5 \qquad [31]$$

should be noted that v_2 and v_2^*, the incident and reflected region 2 shock-frame gas velocities, respectively, are not equal. From Equations [11] and [31], the following relationship for the reflected case initial-shock-frame gas velocity may be derived.

$$v_2^* = u_2(\rho_{52}/(\rho_{52} - 1)) \qquad [32]$$

The application of Equations [10] through [15] to the four-component argon, methane, oxygen and iodine system is given below. The following assumptions are employed: 1) chemical reactions do not occur behind the incident shock wave. 2) The heat of reaction behind the reflected shock wave is negligible, except for the heat from the iodine dissociation reaction which is in equilibrium. The validity of the first assumption lies in the fact that the temperature behind the incident shock wave is generally several hundred degrees lower than the temperature behind the reflected shock wave. The second assumption holds for highly diluted reaction mixtures and for reactions which are not taken far from initial conditions. The iodine dissociation is

rapid compared to the total reaction time and thus may be considered in equilibrium.

In the incident shock-wave case, Equation [16] remains valid for the four-component system, hence Equation [22] may still be used here. In the four-component system, the reaction gas mixture is no longer independent of temperature, thus Equation [17] no longer holds and Equation [30] must be replaced.

If both sides of Equation [26] are divided by P_i and multiplied by ρ_i, Equation [33] results

$$(P_{fi} - 1)((1/\rho_{fi}) + 1) = 2(h_f - h_i)(\rho_i/P_i) \ . \qquad [33]$$

Relations derived from Equations [15] and [16] may be used to substitute for ρ_{fi} and ρ_i/P_i in Equation [33] to yield Equation [34]

$$(P_{fi} - 1)((T_{fi}/P_{fi}) + 1) = (2M/RT_i)(h_f - h_i) \ . \qquad [34]$$

Equation [34] may be rearranged to give Equation [35]

$$P_{fi} + T_{fi} - (T_{fi}/P_{fi}) - 1 = (2/RT_i)(H_f^\circ - H_i^\circ) \ . \qquad [35]$$

Multiplication of Equation [35] by P_{fi} yields Equation [36]

$$P_{fi}^2 + P_{fi}(T_{fi} - (2/RT_i)(H_f^\circ - H_i^\circ) - 1) - T_{fi} = 0 \ , \qquad [36]$$

a second order polynomial in P_{fi}. The appropriate root in Equation [36] is given by Equation [37]

$$P_{fi} = 1/2\{(1 + (2/RT_i)(H_f^\circ - H_i^\circ) - T_{fi}) + [(1 + (2/RT_i)(H_f^\circ - H_i^\circ) - T_{fi})^2 + 4T_{fi}]^{1/2}\} \ . \qquad [37]$$

With Equations [22] and [37], the final state of the region 2 gas behind the incident shock wave for the four-component system may be calculated. It is interesting to note that upon substitution of $(5R/2)(T_f-T_i)$ for $(H_f^\circ - H_i^\circ)$, Equation [37] reduces to Equation [30].

In the reflected shock-wave case, due to the iodine dissociation, Equation [16] no longer holds, thus replacements for Equations [22] and [37] must be derived. The fraction of iodine dissociation, ϕ, is defined as the number of moles of iodine at equilibrium divided by the initial number of moles of iodine. The molecular weights of the region 2 and region 5 gases are given by Equations [38] and [39],

$$M_i = M_2 = M_{Ar}X^\circ_{Ar} + M_{CH_4}X^\circ_{CH_4} + M_{O_2}X^\circ_{O_2} + M_{I_2}X^\circ_{I_2} \qquad [38]$$

$$M_f = M_5 = M_2/(1 + \phi\, X^\circ_{I_2}) , \qquad [39]$$

respectively. The density ratio across the reflected shock is given by Equation [40]

$$\rho_{52} = \rho_{fi} = P_{fi}/(T_{fi}(1 + \phi\, X^\circ_{I_2})) . \qquad [40]$$

The replacements for Equations [22] and [37] may now be derived in the manner described previously to yield the general result: Equations [41] and [42]

$$v_i = [(P_i/\rho_i)(P_{fi} - 1)/(1 - (T_{fi}/P_{fi})(1 + \phi\, X^\circ_{I_2}))]^{1/2} \qquad [41]$$

$$\begin{aligned} P_{fi} = 1/2\{&(1 + (2/RT_i)(H_f^\circ - H_i^\circ) - T_{fi}(1 + \phi\, X^\circ_{I_2})) \\ &+ [(1 + (2/RT_i)(H_f^\circ - H_i^\circ) - T_{fi}(1 + \phi\, X^\circ_{I_2}))^2 \\ &+ 4T_{fi}(1 + \phi\, X^\circ_{I_2})]^{1/2}\} . \end{aligned} \qquad [42]$$

As expected when ϕ is equal to zero, Equations [41] and [42] reduce to Equations [22] and [37], respectively.

The temperature dependence of $(H_f^\circ - H_i^\circ)$ and ϕ can be determined from thermochemical data. The forms of the relationships for these two functions are derived below. With this information, Equations [41] and [42] may be solved by the previously mentioned iterative technique to give a unique determination of state of the gas behind both the incident and reflected shock waves.

To obtain an explicit form for the temperature dependence of the enthalpy, the thermochemical cycle shown in Figure 9 was employed. From Figure 9, Equation [43]

$$H_f^\circ - H_i^\circ = \Delta H^\circ(\text{diss})_f + \Delta H_{fi}^{\circ\prime} = \Delta H^\circ(\text{diss})_i + \Delta H_{fi}^\circ \qquad [43]$$

becomes immediately obvious. Replacement of $\Delta H^\circ(\text{diss})_i$ in Equation [43] by the upper path yields Equation [44]

$$H_f^\circ - H_i^\circ = \Delta H^\circ(\text{diss})_{298} + 2\Delta H^\circ(I)_{i,298} - \Delta H^\circ(I_2)_{i,298} + \Delta H_{fi}^\circ . \qquad [44]$$

An expanded form of Equation [44] is given by Equation [45]

$$H_f^\circ - H_i^\circ = 2\Delta H^\circ(I)_{298} - \Delta H^\circ(I_2)_{298} + 2\Delta H^\circ(I)_{i,298} - \Delta H^\circ(I_2)_{i,298} + \Delta H_{fi}^\circ . \qquad [45]$$

Equation [45] may be rewritten using the integral form of the enthalpy temperature dependence to give Equation [46]

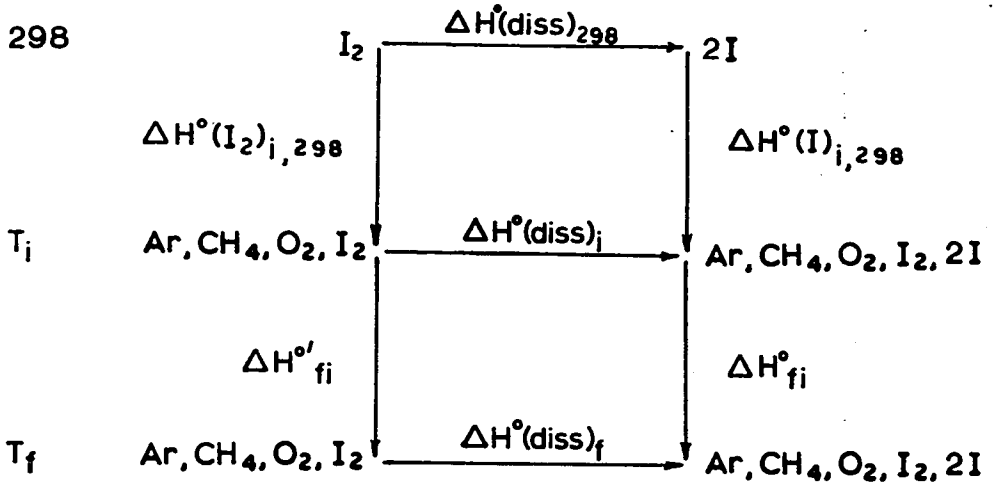

Figure 9. Thermochemical cycle for the dissociation of iodine in the shock tube

$$H_f^\circ - H_i^\circ = [\phi X_{I_2}^\circ (2\Delta H^\circ(I)_{298} - \Delta H^\circ(I_2)_{298}) + 2\phi X_{I_2}^\circ \int_{298}^{i} C_p^\circ(I)dT - (1-\phi)X_{I_2}^\circ \int_{298}^{i} C_p^\circ(I_2)dT + X_{Ar}^\circ \int_{i}^{f} C_p^\circ(Ar)dT + X_{CH_4}^\circ \int_{i}^{f} C_p^\circ(CH_4)dT + X_{O_2}^\circ \int_{i}^{f} C_p^\circ(O_2)dT + (1-\phi)X_{I_2}^\circ \int_{i}^{f} C_p^\circ(I_2)dT + 2\phi X_{I_2}^\circ \int_{i}^{f} C_p^\circ(I)dT]/(1+\phi X_{I_2}^\circ) \quad [46]$$

Values of 1.0685×10^{12} and 6.2442×10^{11} ergs/mole·K were obtained from the JANAF Thermochemical Tables (75) for the standard-state enthalpies of formation of atomic and molecular iodine, respectively. Heat-capacity data for methane, oxygen and iodine were also taken from the JANAF tables. The temperature independent value of $5R/2 = 2.0786 \times 10^{8}$ ergs/mole·K was taken as the heat-capacity function for argon and iodine atoms. The temperature dependence of the fraction of dissociation ϕ is related to the equilibrium constant K_T as shown in Equation [47]

$$\phi = [-K_T/(8X_{I_2}^\circ P_f)] + [(K_T/(8X_{I_2}^\circ P_f))^2 + (K_T/(4X_{I_2}^\circ P_f))]^{1/2} . \quad [47]$$

The application of Equations [41], [42], [46] and [47] to the single-pulsed-shock-tube experiment provides a straightforward method for determining the state of the gas behind the reflected shock wave. A word of caution should be noted at this point. The use of reflected shock waves in kinetics studies involves additional problems.

Reflected shock waves moving back through the growing incident-shock-wave boundary layer cause a strong shock-boundary layer interaction which introduces significant gradients in gas properties in the region 5 gas. In addition, other errors in the measurement of incident shock velocities and in the quenching of region 5 gas may introduce significant uncertainties in the determination of reaction parameters. Due to these problems, large deviations from ideality may occur in reflected-shock-wave experiments. According to Bowman and Hanson (76), single-pulsed-shock-tube experiments are not well suited for quantitative determination of elementary rate coefficients; yet, the technique can be very useful in providing qualitative information on product formation in radical reactions.

EXPERIMENTAL

Chemicals

High-purity helium used as the driver gas in the shock tube, was supplied by the United States Department of the Interior, Bureau of Mines. Argon used as the diluent gas in the reaction end was supplied by Cooks, Inc. and had a minimum purity of 99.99%. Ultra-high-purity methane supplied by Matheson had a minimum purity of 99.97%. Oxygen supplied by Cooks, Inc. had a minimum purity of 99.5%. All gases were used without further purification.

Fisher Scientific Company, A.C.S. certified potassium iodide was made up in a one liter 0.05 M aqueous solution. Carrier free iodine-131 was supplied by International Chemical and Nuclear Corporation. Concentrated iodic acid was prepared by adding an excess amount of Baker's Reagent grade iodic acid to 25 ml of water. Phosphorus pentoxide was supplied by Fisher Scientific Company.

A 5 ml aliquot of potassium iodide was pipetted onto a coarse glass frit. A "spike" of the radioiodine solution was added to the potassium iodide aliquot and a stream of nitrogen gas was bubbled through the solution. Concentrated iodic acid was added dropwise until precipitation of iodine solid was complete. The nitrogen gas was once again bubbled through the solution and the liquid was drawn off. The solid iodine was rinsed with several drops of distilled water, and sublimed through phosphorus pentoxide, then finally collected in a liquid-nitrogen cooled 12 ml sample bulb.

Apparatus

Description of the shock tube and associated electronic instrumentation used for the kinetics experiments is given by Kassman (74). After a storage period of over 10 years, the shock tube originally built and used by Kassman was reassembled and brought into operation; see Figure 10. Original electronic instrumentation used by Kassman to record shock data was repaired and also brought into proper operation. A 3/4" plywood box 12" x 12" x 17' constructed by the Ames Laboratory Maintenance Shop was used to house and protect the shock tube.

The basic operation and tuning procedures of the shock tube remained unchanged, with the following exceptions: (1) the shock tube reaction end was kept at an average temperature of 345 ± 3K, 10K higher than Kassman's temperature. (2) Kassman's filter circuit was discarded and a new electronic filter and delay unit was designed and constructed by the Ames Laboratory Instrumentation Group. The filter-delay unit was placed between the charge amplifier outputs and the oscilloscope inputs. This addition significantly improved the quality of the recorded pressure transient data, see Figure 11. (3) To increase the temperature range of the experiments, 50A Mylar diaphragms were heat treated prior to the experiments. To obtain high-temperature shocks, the diaphragms were placed in the shock tube overnight at approximately room temperature. The temperature was maintained by simply removing the polycarbonate window over the diaphragm section of the shock-tube box and allowing room temperature air to circulate through the diaphragm

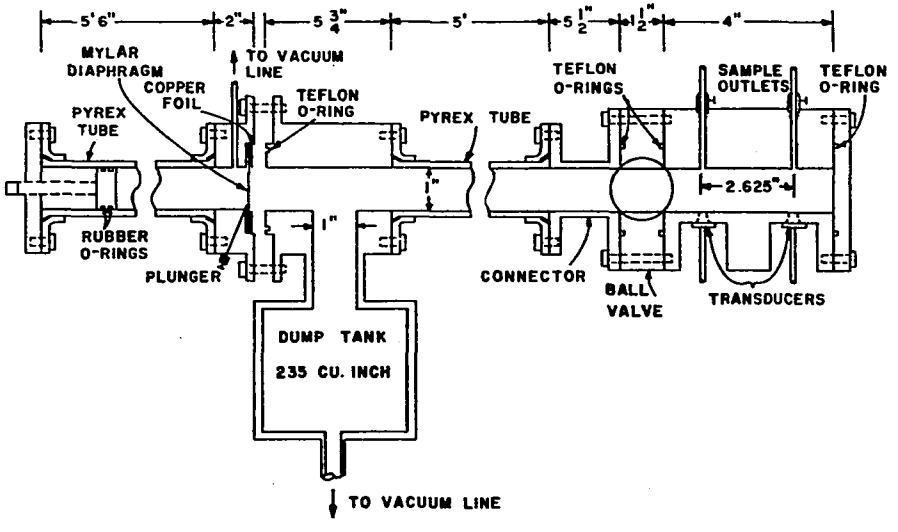

Figure 10. The single-pulse shock tube used for kinetics studies. From Reference (74, p. 54)

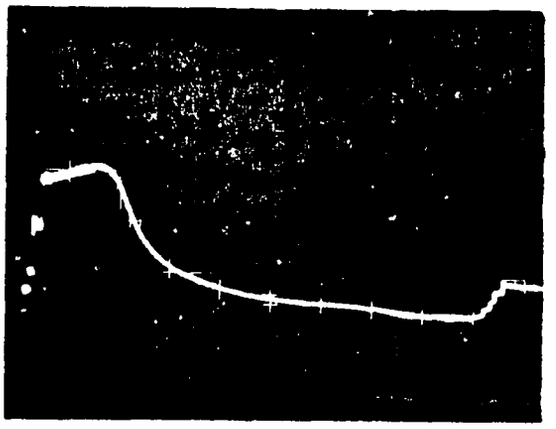

Figure 11a. Recorded output from transducers, voltage (0.5 mV/cm) vs. time (1.0 msec/cm) for a well-tuned shock tube

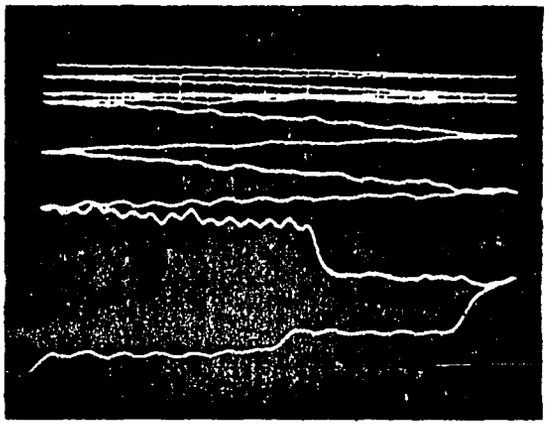

Figure 11b. Raster-sweep photograph of transducer output, with time markers, for a typical shock experiment: $v_1 = 6.82 \times 10^4$ (cm/sec), $v_5 = 3.92 \times 10^4$ (cm/sec), dwell time = 1.34 (msec)

area. The low-temperature shocks were obtained by decreasing the helium-driver-gas pressure from a regulator gauge reading of 34 to 24 psi, and by heat treating the diaphragms in the shock tube overnight at approximately 345K. The temperature was maintained by placing the window over the diaphragm section of the shock-tube box.

A gas-handling system was connected to the sample ports of the reaction end of the shock tube as shown in Figure 12. The storage-tank system and mixing-bulb assembly were evacuated to 10^{-2} torr with rotary pumps. The leak and outgassing rate of the system was less than 10^{-3} torr/min. The shock tube pumped down to 10^{-3} torr with a second rotary pump and had a leak and outgassing rate of less than 10^{-3} torr/min.

Oxygen was admitted to tank #1 and its pressure was read on the Wallace Tiernan Absolute Pressure Gauge. Argon was then admitted to tank #1 and the total pressure was measured on the mercury manometer. The gases were allowed to mix for one day. The absolute pressure gauge and mercury manometer were re-evacuated. Methane was added to tank #2 and its pressure was read on the absolute pressure gauge. The argon-oxygen mixture was allowed to smoothly flow from tank #1 into tank #2, and the resulting pressure was measured on the mercury manometer. Argon was added to tank #2 and total pressure was measured on the mercury manometer. The gasses were allowed to mix for one day.

A freshly prepared sample of iodine solid was weighed out in a 12 ml sample bulb and sublimed into the three liter mixing bulb. The argon-methane-oxygen gas mixture was then admitted into the mixing bulb

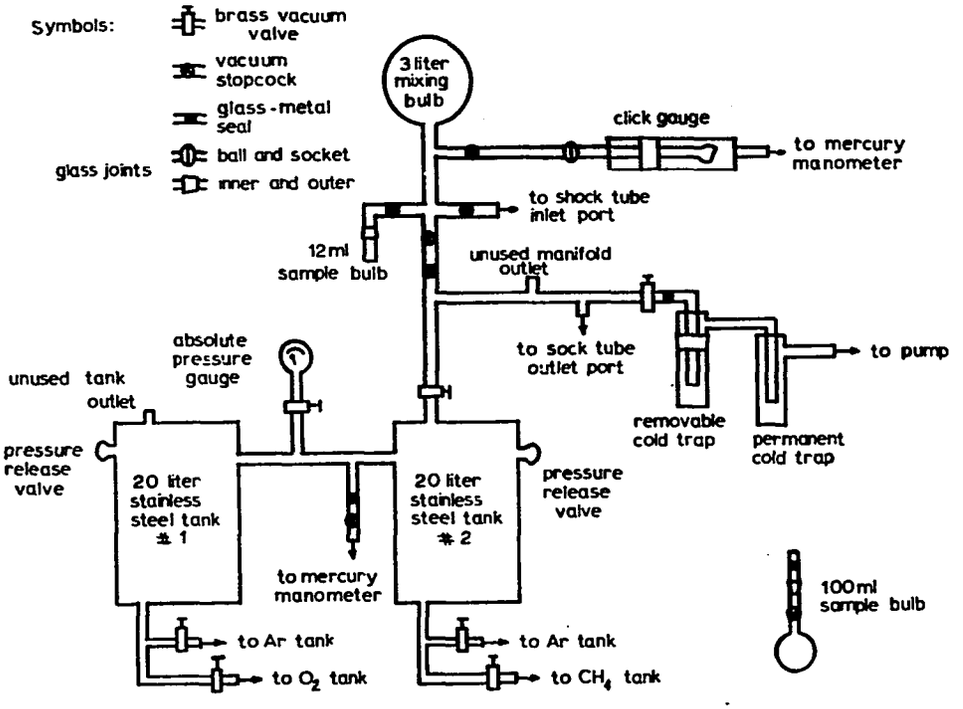

Figure 12. Apparatus used for sample preparation and removal from the shock tube

and the gases were allowed to mix for 12 to 36 hours. The total pressure was measured indirectly through the use of the click gauge. The mixing bulb was maintained at an average temperature of 348 ± 5K, and its volume was determined to be 3121 ± 20 ml. The number of moles of each component in the mixing bulb was calculated using the ideal gas law. The gas mixture was admitted to the shock-tube reaction end and the final pressure was measured again by the use of the click gauge. After the gas mixture was shocked, the products were pumped into the liquid-nitrogen-cooled cold trap.

Procedure

The tuning and operation procedures of the shock tube were the same as described by Kassman (74, p. 61). The frozen products on the removable-outer-cold trap were discarded. The products frozen on the inner tube of the cold trap were dissolved in a 40 ml carbon tetrachloride-iodine-methyl iodide carrier solution contained in a 100 ml test tube. The contents of the test tube were poured into a 250 ml separatory flask. Forty ml of a 0.1 M sodium thiosulfate solution, prepared according to the method described by Skoog and West (77), was poured on top of the carbon tetrachloride solution. The contents of the flask were shaken for approximately 15 seconds. The solution was then allowed to stand for another 30 seconds. The organic phase was drained off into a 50 ml volumetric flask and diluted to volume with carbon tetrachloride. The aqueous phase was drained off into a second 50 ml flask. The 250 ml separatory flask was rinsed with small amounts of

water. The rinsings were added to the aqueous phase, until the 50 ml of volume was obtained. The cold trap was replaced onto the vacuum line and a gas sample from the mixing bulb was taken for analysis, and the entire separation procedure was repeated. It should be noted that care was taken to minimize sample exposure to light during the experiment and separation procedure. It was shown by Harris and Willard (78) that reactions involving iodine and methane, and methyl iodide were photocatalyzed.

Twenty ml aliquots of each sample were pipetted into plastic counting vials. A counting ratio of 1.06 for aqueous to organic solutions was found. All samples were counted on a Tracor Northern 1710 Gamma Ray Spectrum Analyzer. Data on the 364 keV photo peak were automatically corrected for background, detector dead time and Compton scatter by an Automatic Isotope Analysis (AIA) program written for the Tracor Northern 1117 Diskette Memory System. Statistical analysis of data and precalibrated-detector gamma energy efficiency was also handled by the AIA program. An Ortec lithium-drifted germamium crystal was used as the solid-state scintillator. All data were printed out by a Teletype Model 43 deckwriter.

The fraction of reaction, F_{rxn}, was determined using Equation [48]

$$F_{rxn} = [A^{S}_{org}/(A^{S}_{org} + (A^{S}_{aq}/1.06))] - [A^{B}_{org}/(A^{B}_{org} + (A^{B}_{aq}/1.06))] \quad [48]$$

where: A^{S}_{org} = shocked sample organic phase activity,

A^{S}_{aq} = shocked sample aqueous phase activity,

A^{B}_{org} = mixing bulb organic phase activity,

A^{B}_{aq} = mixing bulb aqueous phase activity.

CALCULATIONS

Determination of Reaction Parameters

Least squares fits of the tabulated data from the JANAF Thermochemical Tables (75) for methane, oxygen and iodine heat capacities are given in Table 8. The van't Hoft equation was used by Kassman (74, p. 69) to derive a temperature dependent relationship for the iodine dissociation equilibrium constant in atmospheres, given by Equation [49]

Table 8. Molar heat capacities for CH_4, O_2 and I_2, $C_p^\circ = a + bT + cT^2 + dT^3$ in ergs/mole K

Component	a	b	c	d
CH_4	1.9620×10^8	4.7971×10^5	1.9537×10^2	-1.5232×10^{-1}
O_2	2.5509×10^8	1.3561×10^5	-4.2172×10^1	0
I_2	3.5568×10^8	6.0048×10^4	-5.5455×10^1	-1.8750×10^{-2}

$$\log K_T = 3.824 - (7844/T) + 0.2186 \ln T - 1.53 \times 10^{-5}T + (1858/T^2). \quad [49]$$

The equilibrium constant for the formation of methyl iodide and hydrogen iodide from methane and iodine reported by Goy and Pritchard (70) is given in Equation [50]

$$\log K_{eq} = 0.759 - (2768.5/T). \qquad [50]$$

A PL-1 program for the Iowa State Computer Center ITEL AS6 computer was written to calculate the state of the gas behind the reflected shock wave from the initial conditions and the reflected shock velocity. The following is a brief description of the program's method.

Input data, initial conditions and guesses for the temperature and pressure ratios across the shock waves were entered. The region 2 conditions were calculated first. The selected value of T_2 was used to calculate the enthalpy change, and Equation [37] was used to obtain a value for P_{21}. The shock wave velocity v_1 was then calculated from Equation [20]; this value was compared with the measured incident shock velocity. The selected value of T_{21} was adjusted accordingly and the process was repeated until sufficient accuracy between calculated and measured incident shock velocities was obtained.

Once the region 2 gas state had been determined, the experimental value of u_2 was calculated by use of Equation [31]. The selected values of P_5 and T_5 were used to calculate K_T, via Equation [49]. Next, ϕ and $H_f^\circ - H_i^\circ$ were calculated from Equations [47] and [46], respectively. Equation [42] was used to obtain a value for P_{52}. Then v_2^* was calculated by use of Equation [41]. From the current values of P_{52}, T_{52} and ϕ, D_{52} was obtained from Equation [40] and a trial value of v_2^* was calculated by means of Equation [32]. The calculated and trial values of v_2^* were compared, and the selected value of T_{52} was adjusted to improve the agreement. The current value of P_{52} was obtained from the

calculated result of Equation [42] and the process was repeated until the difference between the calculated and trial values of v_2* were less than a designated value.

A second computer program was written by Dr. Martin for the Texas Instrument-59 calculator. The equations used in the TI-59 program were independently derived, and a different iterative technique was employed. Results from the PL-1 program and the TI-59 program differed by no more than 3K for the final calculation of T_5. This difference, well within the experimental uncertainty of ± 25K, was attributed to the fact that Dr. Martin fit his heat capacity functions to only four data points, while the heat capacity functions given in Table 8 were fit by least squares to ten data points spaced at 100K intervals over the entire range of experimental temperatures, e.g., 300 to 1200K.

The measured incident shock velocity was taken as the time between the first two pressure rises, measured from Figure 11b, divided into the distance between the transducers, 6.6675 cm. The time between the final pressure rise to the arrival of the cooling wave, measured from Figure 11b, was taken as the observed dwell time.

Figure 13 contains an enlargement of the reaction zone corresponding to region 5 in Figure 8. The gases taken for analysis were those between the ball valve and endplate. The average reaction time in the sample of region 5 gas taken for analysis was approximated by Equation [51]

$$t_{ave} = t_{obs} + [(1/v_5) + (1/a_5)]X_o \qquad [51]$$

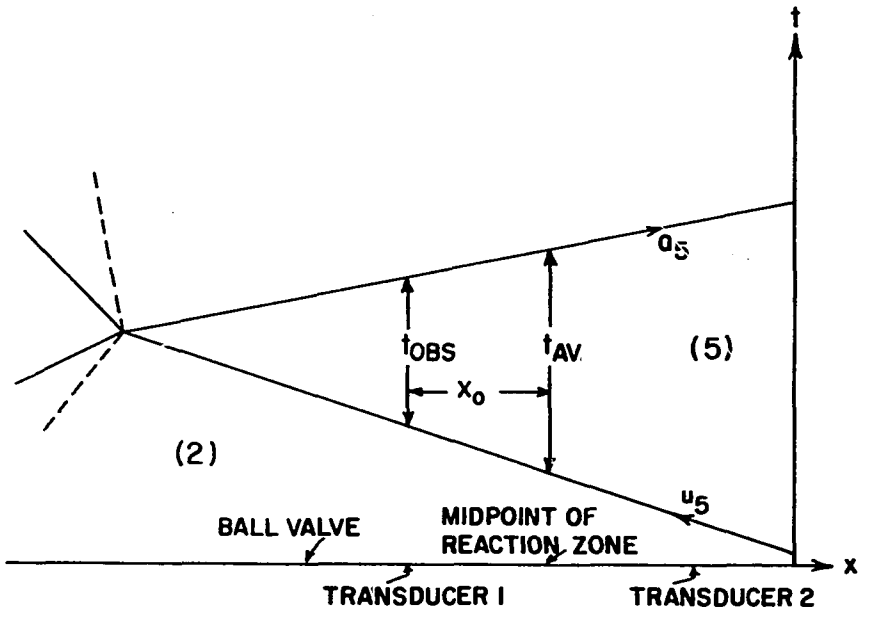

Figure 13. Enlargement of the reaction zone in the shock tube, represented in x-t space. From Reference (74, p. 74)

where: t_{obs} = the observed dwell time in seconds,

v_5 = calculated reflected shock velocity in cm/sec,

a_5 = the region 5 speed of sound in cm/sec,

X_o = the distance from transducer 1 to the midpoint of the reaction zone, 3.3338 cm.

The reflected shock velocity, v_5, was determined from the region 5 gas conditions and the use of Equation [11]. Equation [10] was used to determine the value of a_5, in which γ was given by Equation [52]

$$\gamma = C_p^\circ/(C_p^\circ - R) \quad . \qquad [52]$$

Derivation of Rate Equations

The mechanistic scheme for the formation of methyl iodide from methane and iodine is given by Reactions (39), (40), (41), (22), (42) and (43). The rate of formation of methyl iodide is given by Equation [53]

$$\frac{d(CH_3I)}{dt} = k_{41}(CH_3)(I_2) - k_{41}(CH_3I)(I) + k_{42}(CH_3)(I)(M) \quad . \qquad [53]$$

The steady-state assumption for the methyl-radical may be used to obtain Equation [54]

$$\frac{d(CH_3I)}{dt} = k_{40}(CH_4)(I)\left[1 + \frac{k_{42}(M)(I)}{k_{41}(I_2)} - \frac{1}{K_{eq}}\frac{(CH_3I)(HI)}{(CH_4)(I_2)}\left[1 + \frac{k_{22}(CH_3)}{k_{-40}(HI)}\right]\right] \div \left[1 + \frac{k_{-40}(HI) + k_{22}(CH_3) + k_{42}(M)(I)}{k_{41}(I_2)}\right] \quad . \qquad [54]$$

Reaction (41) is the most rapid reaction in the mechanism; thus, in the presence of excess iodine, the methyl radical concentration remains several orders of magnitude below product concentration levels, and $k_{-40}(HI) \gg k_{22}(CH_3)$. Also, when $(HI)_o \ll (I_2)_o$, $k_{41}(I_2) \gg k_{-40}(HI)$; and finally $k_{41}(I_2) \gg k_{42}(M)(I)$. Thus, Equation [54] reduces to the simpler form, Equation [55]

$$\frac{d(CH_3I)}{dt} = k_{40}(CH_4)(I)\left[1 - \frac{1}{K_{eq}}\frac{(CH_3I)(HI)}{(CH_4)(I_2)}\right] . \qquad [55]$$

This result indicates that under the above reaction conditions, Reactions (22) and (42) may be omitted from the mechanism.

In the kinetics experiments presented in this work, the formation of methyl iodide was never greater than 10% of its equilibrium value; consequently, Equation [55] reduces to Equation [56]

$$\frac{d(CH_3I)}{dt} = k_{40}(CH_4)(I) . \qquad [56]$$

The rate of decomposition of iodine is given by Equation [57]

$$\frac{d(I_2)}{dt} = k_{43}(I)^2(M) - k_{39}(I_2)(M) + k_{-41}(CH_3I)(I) - k_{41}(CH_3)(I_2) \qquad [57]$$

Once again, by use of the steady-state assumption for the methyl radical, and by use of the previous assumptions concerning the formation of methyl iodide, Equation [58]

$$\frac{d(I_2)}{dt} = k_{43}(I)^2(M) - k_{39}(I_2)(M) - k_{40}(CH_4)(I) \qquad [58]$$

may be derived. The rate constants for Reactions (43) and (39) reported by Britton et al. (72) are given in Equations [59] and [60],

$$k_{43} = 10^{14.87}(1000/T)^{1.9}\ cm^6/mole^2\ sec, \quad [59]$$

$$k_{39} = 1.5 \times 10^{10}\ T^{1/2}(35{,}544/RT)^{2.83}\ \exp(-35{,}544/RT)\ cm^3/mole\ sec \quad [60]$$

respectively. The rates of iodine dissociation and iodine atom recombination are much greater than the rate of Reaction (40); therefore, Equation [58] may be rewritten as Equation [61]

$$\frac{d(I_2)}{dt} = k_{43}(I)^2(M) - k_{39}(I_2)(M)\ . \quad [61]$$

The solution to Equation [61] is given by Equation [62]

$$2[(I_2)_o - (I_2)_t] = (I)_t = (I)_{eq}\left[\frac{1 - \exp(-k_{43}(M)Gt)}{1 + H\exp(-k_{43}(M)Gt)}\right] \quad [62]$$

where: $G = [K^2 - 16K(I_2)_o]^{1/2}$,

$K = k_{39}/k_{43}$,

$H = (G-K)/(G+K)$.

Substitution of $(I)_t$ from Equation [62] into Equation [56] followed by integration from t=0 to $t=t_{ave}$ yields Equation [63]

$$\Delta(CH_3I) = k_{40}(CH_4)_o(I)_{eq}\left[t_{ave} + \left(\frac{1}{2k_{43}(M)(I)_{eq}}\right)\ln\left(\frac{1 + H\exp(-k_{43}(M)Gt_{ave})}{1 + H}\right)\right], \quad [63]$$

with the assumption that the methane, iodine and iodine atom concentrations are not significantly affected by the formation of small

amounts of methyl iodide. This result indicates that the rate of formation of methyl iodide was determined mainly by the rate of the chain-initiation step of the free-radical mechanism. Due to the fact that the average reaction times were quite short, the rate of the iodine dissociation was included in the calculation of k_{40}; afterwards, it was found that the iodine equilibrium was effectively established in 5 to 50% of the total reaction time. Since the experimentally determined rate constant is known by no better than a factor of 2, corrections of this type are questionable. Thus, the simple linear approximation for the formation of methyl iodide given by Equation [64]

$$k_{40} = \frac{\Delta(CH_3I)}{(CH_4)_o(I)_{eq}t_{ave}} \text{ cm}^3/\text{mole sec} \qquad [64]$$

was used to calculate the rate constant for Reaction (40).

Once the system had been calibrated for the rate of the methane-iodine reaction over the experimental temperature range, oxygen was added to the methane-iodine reaction mixture. The following reactions were used to describe the mechanism:

$$I_2 + M \rightarrow I + I + M \qquad (39)$$

$$CH_4 + I \rightleftarrows CH_3 + HI \qquad (40)$$

$$CH_3 + I_2 \rightleftarrows CH_3I + I \qquad (41)$$

$$I + I + M \rightarrow I_2 + M \qquad (43)$$

$$CH_4 + O_2 \rightarrow CH_3 + HO_2 \qquad (2)$$

$$CH_4 + HO_2 \rightarrow CH_3 + H_2O_2 \qquad (16)$$

$$CH_3 + O_2 \rightarrow CH_2O + OH \qquad (4)$$

$$CH_4 + OH \rightarrow CH_3 + H_2O \quad (13)$$

$$HO_2 + I_2 \rightarrow HI + IO_2 \quad (44)$$

$$CH_2O + I \rightarrow HCO + HI \quad (45)$$

$$HCO + O_2 \rightarrow CO + HO_2 \quad (46)$$

$$HCO + I \rightarrow CO + HI \quad (47)$$

The measured change in the rate of methyl iodide production, due to the addition of oxygen to the reaction mixture, was used to determine an upper limit for the methane-oxygen initiation reaction.

The rate of formation of methyl iodide is given by Equation [64]

$$\frac{d(CH_3I)}{dt} = k_{41}(CH_3)(I_2) - k_{-41}(CH_3I)(I) \quad [65]$$

The change of the methyl radical concentration with respect to time is given by Equation [66]

$$\frac{d(CH_3)}{dt} = k_{40}(CH_4)(I) + k_{-41}(CH_3I)(I) + k_2(CH_4)(O_2) + k_{16}(CH_4)(HO_2) + k_{13}(CH_4)(OH) - (CH_3)[k_{-40}(HI) + k_{41}(I_2) + k_4(O_2)] . \quad [66]$$

By use of the steady-state assumption for the methyl, hydroxyl and hydroperoxyl radicals, Equation [65] may be rearranged to give Equation [67]

$$(CH_3) = \left(\frac{1}{k_{-40}(HI) + k_{41}(I_2)}\right)\left[k_{40}(CH_4)(I) + k_{-41}(CH_3I)(I) + k_2(CH_4)(O_2) + k_{16}(CH_4)\left[\frac{k_2(CH_4)(O_2) + k_{46}(O_2)\left(\frac{k_{45}(I)(CH_2O)}{k_{46}(O_2) + k_{47}(I)}\right)}{k_{16}(CH_4) + k_{44}(I_2)}\right]\right] . \quad [67]$$

The steady-state concentration of methyl radicals would remain low in the presence of oxygen and excess iodine. Consequently, elimination of Reaction (22) and (42) from the mechanism is still valid. Although it should be noted that at higher temperatures and larger methyl-radical-production rates, Reaction (22) should begin to successfully compete with Reaction (41) for methyl radicals. Reaction (32) was excluded from the mechanism because at reaction conditions, its equilibrium lies far to the reactants side. Reaction (5) is probably too slow to compete with Reaction (4) at lower temperatures. The decomposition of formaldehyde via Reaction (7), because of its 72 kcal/mole activation energy, may be omitted from the mechanism also.

The uncertainty in the rate of Reaction (4) makes it difficult to estimate exactly how well this process competes with iodine for methyl radicals. In any case, the hydroxyl radical formed by Reaction (4) rapidly reacts with the excess methane present in the system via Reaction (13) to produce a methyl radical and a molecule of water. Therefore, as seen in Equation [67], Reaction (4) does not affect the methyl-radical steady-state concentration, yet Reaction (4) must still be included in the mechanism since it serves to deplete the oxygen concentration.

The relative rates of Reactions (16) and (44) are difficult to assess, but in the presence of a large excess of methane, the abstraction of a proton from methane by the hydroxyl radical is probably a more rapid reaction than the four-center iodine-hydroperoxyl radical reaction. Consequently, it was assumed that $k_{16}(CH_4) \gg k_{44}(I_2)$.

The rate of Reaction (45) depends upon the formaldehyde concentration which remains quite low because of the slow rate of Reaction (4) relative to Reaction (41). The build up of formaldehyde in the reaction mixture is limited by the presence of oxygen and iodine atoms via Reactions (46) and (47), respectively. Because very small amounts of formaldehyde were found, formyl radical concentration levels remained quite low. Although the determination of the formyl radical concentration was not possible in this work, it was assumed that the rate of formaldehyde decomposition followed by the subsequent formation of carbon monoxide remained insignificant throughout the course of the experiment.

With the above conclusions, the steady-state methyl radical concentration is now given by Equation [68]

$$(CH_3) = [k_{40}(CH_4)(I) + k_{-41}(CH_3I)(I) + 2k_2(CH_4)(O_2)] \div [k_{-40}(HI) + k_{41}(I_2)] \cdot \qquad [68]$$

This result indicates that in the presence of excess iodine under conditions of low temperatures and short reaction times, Reactions (44) through (47) may be omitted from the mechanism.

Substitution of (CH_3) from Equation [68] into Equation [65] yields Equation [69]

$$\frac{d(CH_3I)}{dt} = [k_{40}(CH_4)(I)\left\{1 - \frac{1}{K_{eq}}\frac{(CH_3I)(HI)}{(CH_4)(I_2)}\right\} + 2k_2(CH_4)(O_2)] \div \left[1 + \frac{k_{-40}(HI)}{k_{41}(I_2)}\right] \cdot \qquad [69]$$

By use of the assumptions applied to the methane-iodine reaction, Equation [69] may be reduced to Equation [70]

$$\frac{d(CH_3I)}{dt} = k_{40}(CH_4)(I) + 2k_2(CH_4)(O_2) \ , \qquad [70]$$

which, upon integration, yields the expression for k_{40} given by Equation [71]

$$k_{40} = k_{40'} - 2k_2 \frac{(O_2)_o}{(I)_{eq}} \ cm^3/mole \ sec \qquad [71]$$

where: $k_{40'} = \dfrac{\Delta(CH_3I)'}{(CH_4)_o(I)_{eq} \ t_{ave}} \ cm^3/mole \ sec.$

Rearrangement of Equation [71] yields the following expression for k_2:

$$k_2 = (k_{40'} - k_{40}) \frac{(I)_{eq}}{2(O_2)_o} \ cm^3/mole \ sec. \qquad [72]$$

In the radiochemical experiments, the increase in activity in the organic phase was used to follow the progress of the reaction. Since the specific activities of the organic and inorganic iodine products were equal, the mole fraction of the methyl iodide was readily determined from the known quantities, F_{rxn} and $X^{\circ}_{I_2}$, as shown in Equation [73]

$$X^{\circ}_{CH_3I} = 2X^{\circ}_{I_2} F_{rxn} \qquad [73]$$

Hence, in terms of the region 5 gas-dynamic variables, Equations [64] and [72] may be rewritten as Equations [74] and [75], respectively,

$$k_{40} = \frac{F_{rxn}}{C_5 \, X^{\circ}_{CH_4} \, \phi \, t_{ave}} \ cm^3/mole\ sec, \qquad [74]$$

where: $C_5 = \frac{P_5}{RT_5(1 + \phi X^{\circ}_{I_2})}$ mole/cm^3,

$$k_2 = (k_{40'} - k_{40}) \frac{\phi X^{\circ}_{I_2}}{X^{\circ}_{O_2}} \ cm^3/mole\ sec. \qquad [75]$$

Contained within this set of data is information concerning the rate of formaldehyde formation. From Reaction (4), and by use of the steady-state approximation for the methyl radical given in Equation [68], Equation [76]

$$\frac{d(CH_2O)}{dt} = \frac{k_4(O_2)}{k_{41}(I_2)} k_{40}(CH_4)(I)\left[1 + \frac{k_{-41}(CH_3I)}{k_{40}(CH_4)} + \frac{2k_2(O_2)}{k_{40}(I)}\right] \qquad [76]$$

may be derived. Under the experimental conditions presented in this work, $k_{40}(CH_4) >> k_{-41}(CH_3I)$ and $k_{40}(I) >> 2k_2(O_2)$, consequently, Equation [76] reduces to Equation [77]

$$\frac{d(CH_2O)}{dt} = \frac{k_4(O_2)}{k_{41}(I_2)} k_{40}(CH_4)(I) \qquad [77]$$

which upon integration yields the following expression for the Reaction (4) rate constant:

$$k_4 = k_{41} \frac{(I_2)_{eq}}{(O_2)_o} \frac{\Delta(CH_2O)}{\Delta(CH_3I)} \ cm^3/mole\ sec\ . \qquad [78]$$

Thus, the simultaneous single-experiment determination of the formaldehyde and methyl iodide changes in concentration would yield an estimate of the Reaction (4) rate constant.

A more complete and accurate analysis of the proposed methane-oxygen-iodine mechanistic scheme would require the use of a numerical-integration technique such as a fourth-order Runge-Kutta (79) (or one of several other methods described by Gear (80)) to solve for the unknown rate constants and determine the concentration vs. time profiles of the reacting species. Since the data presented in this work were not suitable for such an in-depth analysis, this procedure was not attempted.

RESULTS AND DISCUSSION

Results from the methane-iodine and the methane-oxygen-iodine experiments are contained in Tables 9, 10 and 11. The data listed in Tables 9 and 10 were obtained from the radio-iodine analytical technique. The data included in Table 11 were obtained from mass-spectral analysis of the reaction samples.

The initial pressures are tabulated in the second column. The measured incident shock velocities are given in the third column. The concentrations of methane, oxygen and iodine in argon are listed in the succeeding columns. Contained in the next column is the fraction of reaction (Tables 9 and 10) or the ratio of peak heights (Table 11) observed in each experiment. The next four columns contain the calculated parameters, pressure, temperature, molar density and fraction of iodine dissociation, obtained by the application of the ideal-shock-tube theory to the reaction mixture. The average reaction times are listed in the second to the last column. The logarithm of the observed rate constant, k_{40} for the methane-iodine reaction mixtures and k'_{40} for the methane-oxygen-iodine reaction mixtures, is listed in the final column.

The experimentally observed values for the rate of methyl iodide formation are plotted in Figure 14, along with the low-temperature work of Goy and Pritchard (70) and Golden *et al.* (81). Also shown in Figure 14 is the least squares fit (82) of the low-temperature work of Goy and Pritchard and Golden *et al.* extrapolated to the higher temperatures relevant to the present work.

Table 9. Details of the CH_4 + I_2 radio-iodine experiments

Exp. No.	P_1 (mm)	Inc. shock vel. (km/sec)	CH_4 conc. mole %	I_2 conc. mole %	$F_{rxn} \times 10^2$	P_5 (mm)	T_5 (K)	$C_5 \times 10^5$ $\left(\frac{mole}{cm^3}\right)$	$\phi \times 10^2$	t_{ave} (msec)	log k_{40} $\left(\frac{cm^3}{mole\ sec}\right)$
1	186	0.657	3.43	0.139	1.22	2372	1028	3.70	40.9	1.70	7.14
2	172	0.671	3.56	1.217	1.06	2371	1063	3.67	43.2	1.51	7.11
3	172	0.678	3.56	0.216	0.690	2450	1080	3.63	47.2	1.56	6.86
4	210	0.634	2.57	0.183	0.656	2407	984	3.92	26.3	2.05	7.08
5	176	0.645	2.57	0.211	0.384	2133	1011	3.38	32.1	1.78	6.89
6	148	0.667	2.57	0.199	2.12	1995	1067	2.99	48.4	1.49	7.58
7	144	0.680	2.57	0.245	0.385	2078	1101	3.03	53.3	1.55	6.78
8	198	0.601	3.02	0.176	2.53	1888	894	3.38	12.9	2.01	7.98
9	180	0.608	3.02	0.191	0.518	1785	912	3.14	15.3	1.86	7.28
10	155	0.659	3.02	0.218	1.68	2026	1040	3.12	39.5	1.84	7.39
11	173	0.652	2.03	0.195	1.43	2160	1036	3.34	39.3	1.78	7.48
12	181	0.618	2.03	0.208	2.13	1912	948	3.21	20.3	1.89	7.93
13[a]	239	0.570	3.51	0.150	0.519	1898	815	3.73	5.32	2.47	7.48
14	212	0.608	3.51	0.130	0.802	2095	906	3.71	16.0	2.09	7.27
15	184	0.612	3.51	0.208	0.905	1869	917	3.27	15.1	1.94	7.43
16	168	0.652	3.51	0.215	0.905	2108	1017	3.32	33.6	1.91	7.08

17[b]	238	0.576	2.00	0.151	0.367	1963	842	3.71	7.44	2.36	7.45
18	201	0.583	2.00	0.176	2.25	1735	859	3.21	9.08	2.06	8.27
19	184	0.623	2.00	0.178	1.43	1983	960	3.28	23.7	2.02	7.66
20	158	0.648	2.00	0.222	2.64	1952	1027	3.02	36.7	1.63	7.86
21[b]	203	0.648	2.00	0.176	0.667	2496	1026	3.87	36.5	1.76	7.13
22	161	0.676	2.00	0.211	7.61	2272	1100	3.28	54.3	1.50	8.15
23	142	0.695	2.00	0.227	10.6	2194	1151	3.03	66.2	1.39	8.28

[a]If the data had been corrected for the iodine dissociation time, this experiment would have had the largest correction, and the t_{ave} value 2.47 msec would have been lowered to 1.26 msec.

[b]In this experiment, F_B was between 70 and 80% of F_S.

Table 10. Details of the $CH_4 + O_2 + I_2$ radio-iodine experiments

Exp. No.	P_1 (mm)	Inc. shock vel. (km/sec)	CH_4 conc. mole %	O_2 conc. mole %	I_2 conc. mole %	$F_{rxn} \times 10^2$	P_5 (mm)	T_5 (K)	$C_5 \times 10^5$ $\left(\frac{mole}{cm^3}\right)$	$\phi \times 10^2$	t_{ave} (msec)	log k'_{40} $\left(\frac{cm^3}{mole\ sec}\right)$
1	241	0.587	2.03	0.180	0.156	1.07	2131	871	3.89	9.97	2.47	7.74
2	207	0.602	2.03	0.180	0.174	1.84	2003	909	3.50	14.7	2.21	7.90
3	184	0.635	2.03	0.180	0.185	0.548	2113	990	3.39	29.3	2.12	7.11
4	162	0.661	2.03	0.180	0.215	0.989	2132	1056	3.21	43.8	1.80	7.28
5	237	0.599	1.99	0.223	0.159	1.22	2237	898	3.96	13.1	2.03	7.76
6	207	0.630	1.99	0.223	0.156	1.21	2319	977	3.77	27.2	1.89	7.50
7	184	0.661	1.99	0.223	0.190	3.37	2409	1058	3.62	43.9	1.58	7.83
8	162	0.684	1.99	0.223	0.239	6.81	2379	1121	3.37	56.5	1.37	8.11
9	137	0.692	1.99	0.223	0.299	12.1	2107	1143	2.93	60.3	1.28	8.43
10[a]	234	0.573	2.04	0.381	0.150	1.15	1906	835	3.63	6.92	2.57	7.94
11	205	0.587	2.04	0.381	0.176	1.94	1816	869	3.32	9.95	2.18	8.12
12	182	0.593	2.04	0.381	0.202	0.894	1674	885	3.01	11.6	2.12	7.77
13	157	0.641	2.04	0.381	0.218	2.32	1869	1005	2.96	32.3	1.78	7.82
14	180	0.652	2.02	0.376	0.130	1.07	2254	1033	3.47	44.0	1.59	7.34

[a] In this experiment, F_B was 49% of F_S.

Table 11. Details of the $CH_4 + I_2$ and $CH_4 + O_2 + I_2$ mass-spectral experiments

Exp. No.	P_1 (mm)	Inc. shock vel. (km/sec)	CH_4 conc. mole %	O_2 conc. mole %	I_2 conc. mole %	r_{rxn}[a] $\times 10^4$	P_5 (mm)	T_5 (K)	$C_5 \times 10^5$ $\left(\frac{\text{mole}}{\text{cm}^3}\right)$	ϕ $\times 10^2$	t_{ave} (msec)	log k'_{40} $\left(\frac{\text{cm}^3}{\text{mole sec}}\right)$
1	192	0.659	1.97	---	0.176	18.6	2506	1057	3.78	44.3	1.63	7.29
2	159	0.686	1.97	---	0.202	40.9	2359	1128	3.34	61.4	1.39	7.55
3	218	0.583	2.01	---	0.158	0.481	1873	859	3.48	9.19	2.43	6.30
4	233	0.572	1.73	0.390	0.099	0.526	1868	833	3.58	8.32	2.42	6.56
5	196	0.625	1.73	0.390	0.154	0.630	2146	968	3.54	26.4	1.92	6.06
6	143	0.702	1.73	0.390	0.168	99.7	2268	1176	3.08	76.0	1.29	7.99
7	136	0.682	1.99	3.86	0.233	116.0	1988	1097	2.89	54.1	1.17	8.13

[a] $r_{rxn} = r_S - r_B$, where r is the ratio of the methyl iodide (mass 142) peak height to the methane (mass 16 + mass 15) peak height, corrected for relative sensitivity; thus, $k_{40} = r_{rxn}/(C_5\ 2\phi X^{\circ}_{I_2}\ t_{ave})$.

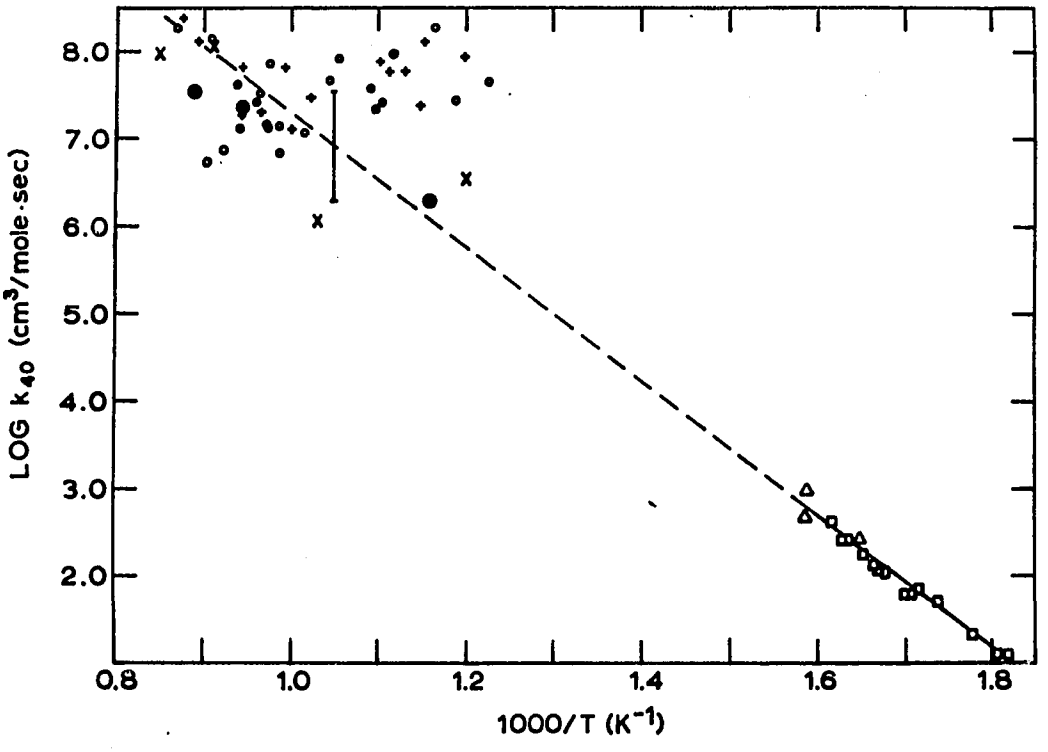

Figure 14. Arrhenius plot of the rate of methyl iodide formation:

- o present work $CH_4 + I_2$ radio-iodide experiments,
- ● present work $CH_4 + I_2$ mass-spectral experiments,
- \+ present work $CH_4 + O_2 + I_2$ radio-iodine experiments,
- x present work $CH_4 + O_2 + I_2$ mass-spectral experiments,
- □ Reference (70),
- △ Reference (81)

The pre-Arrhenius and activation energy parameters, determined from the low-temperature results reported by Goy and Pritchard and Golden et al., were $A = 10^{15.1\pm0.53}$ cm^3/mole sec and $E = 35.45\pm1.44$ kcal/mol, respectively. The estimation of the range in the extrapolated value of the rate constant at 950K was found to be log $k_{40}(cm^3/mole\ sec) = 6.9\pm0.63$, as plotted in Figure 14.

Radio-iodine Experiments

The shock-tube, ratio-iodine results were scattered about the extrapolated low-temperature line. Although the high-temperature shock data, for the most part, fell within the extrapolated error in log k_{40}, the low-temperature log k_{40} values were quite noticeably too high.

After the first sixteen methane-iodine experiments were performed, fourteen methane-oxygen-iodine experiments were completed. Then, a second set of methane-iodine experiments was carried out.

The first two methane-iodine shock experiments which were near to 1100K, namely Experiments 3 and 7 of Table 9, gave log k_{40} values which fell well below the other high-temperature experiments and outside of the extrapolated error in the low-temperature results of Goy and Pritchard and Golden et al.

The high-temperature results in the second set of methane-iodine experiments fell within the extrapolated, low-temperature data. The high-temperature results for the methane-oxygen-iodine shock experiments fell within the error of the experiment and were also scattered about the extrapolated, low-temperature line.

The low-temperature log k'_{40} results were also consistently high for the methane-oxygen-iodine shock experiments.

The methane, iodine, and oxygen concentrations were varied slightly from experiment to experiment: methane ranged between 1.99 and 3.56 mole percent, iodine ranged between 0.099 and 0.299 mole percent, and oxygen ranged between 0.00 and 3.86 mole percent. Safety considerations prevented the use of high concentrations of methane and oxygen. On the other hand, significant concentrations of methane were required since the amount of methyl iodide formation was quite low. Because iodine had to be weighed analytically, a lower limit on its concentration was encountered. The upper limit of the I_2 concentration was determined by the radiation hazard and low vapor pressure of iodine. Due to the limited range of concentrations, determination of individual reaction orders was not possible. In addition, this small degree of variation in concentration would not be expected to account for the large range of log k_{40} values found in the high-temperature shock experiments, namely Experiments 3 and 7 compared with Experiments 22 and 23 of Table 9.

The F_{rxn} determined by the radiochemical technique was found by analysis of the shocked sample and the mixing-bulb sample for a given experiment. In each experiment, the shocked-sample fraction of reactivity, F_S, was found to be greater than the bulb-sample fraction of activity, F_B.

Although F_B was not measured for the first thirteen methane-iodine experiments, it was measured in each of the following radio-iodine

experiments, and it was found that F_B was 35% of F_S or less, with one-half of the F_B values less than 20% of F_S. Thus, this correction was less than the overall error of the experiment. It should be noted that three exceptions were found, namely, Experiments 17 and 21 on the methane-iodine mixtures in which F_B was found to be 78 and 71% of F_S, respectively, and in Experiment 10 on the methane-oxygen-iodine mixtures in which F_B was 49% of F_S. A distinct oxygen effect on the F_B value was not observed.

Certainly, the amount of methyl iodide found in the mixing bulb was not large enough to significantly effect the calculation of the Reaction (40) rate constant, yet, the F_B values were greater than expected. The formation of methyl iodide in the mixing bulb was attributed to the photo-catalyzed reactions described by Harris and Willard (78). Care was taken to reduce the exposure of visible light to the mixing bulb, yet no attempt was made to determine the magnitude of exposure. It was also noted that the F_B values exhibited a general increase from one set of experiments to the next. Whereas, the F_B values averaged around 1×10^{-3} for the earlier experiments, the F_B values rose to approximately 5×10^{-3} for the final set of radio-iodine experiments. The largest F_B value, 1.6×10^{-2}, was found in Experiment 21 of the methane-iodine experiments.

The significance of the above findings is not certain. Several factors, or any combination thereof, were postulated to be the cause of the anomalies in these results.

Nonideal shock dynamics at lower temperatures could have contributed to the high log k_{40} and log k'_{40} values found below 950K. At slower incident shock speeds and longer contact times, growth of the boundary layer in the region 2 gas would have caused the conditions behind the reflected shock wave to significantly deviate from ideality.

Also, uncertainty in the calculated value of the reaction temperature, T_5, was a major cause of the large degree of scatter found in both the high and low temperature shock experiments.

A reaction at higher temperatures which consumed methyl iodide but did not lead to the formation of other organic iodides was considered as a possible explanation for the apparent lack of increase in the rate of Reaction (40) with temperature. Reaction (48),

$$CH_3I + CH_4 = C_2H_6 + HI \qquad (48)$$

the formation of ethane and hydrogen iodide from methyl iodide and methane, was proposed as a possible candidate to describe the above effect. Of course, the immediate objection to this consideration is that eventually the ethane formed in Reaction (48) would begin to react with the excess iodide in the system to produce organic iodide in the form of ethyl iodide. By use of the enthalpies of formation for methane and ethane reported by Moore (83), hydrogen iodide reported in the JANAF Tables (75) and methyl iodide reported by Goy and Pritchard (70), $\Delta H^\circ_{f,298}$ for Reaction (48) was estimated to be 0.6 kcal/mole.

The sampling and radio-analytical technique may have affected the determination of both F_S and F_B. As was mentioned previously, the

exposure to light during any step of the analysis could have affected the methyl iodide concentration. Also, the solvent extraction technique could have allowed for some exchange between I^- and CH_3I to occur. Tests were made on the separation procedure. A "spike" of iodine-131 in the form of I_2 was introduced into a carrier solution and the separation procedure was performed. Between 0.01 and 0.10% of the activity was found in the organic phase. The fraction of activity found in the organic phase increased with the concentration of methyl iodide carrier and with the visible-light exposure time.

The method used for sampling was questioned. The loss of I_2 by reaction with stopcock grease and with the metal parts of the vacuum system may have had a significant effect on the results. No attempt was made to determine the actual extent of this error.

The fraction of activity found in the bulb varied from a low value of 5×10^{-4} found in Experiment 9 of Table 10 to a high value of 1.6×10^{-2} found in Experiment 21 of Table 9. In Experiment 22 of Table 9, F_B was found to be 4×10^{-3}; this reaction mixture was stored under nearly identical conditions as the previous experiment. Thus, it may be seen that the fraction of activity values were not more accurate than $\pm 5 \times 10^{-3}$ with a background level varying between 1×10^{-4} to 1×10^{-3}. The magnitude of these uncertainties could have been extremely significant in the determination of F_{rxn} values at 1×10^{-3} or less in the low-temperature shock experiments. It still must be stated that for a given experiment the F_S value was always found to be greater than the F_B value.

The general trend of increase in F_B value from experiment to experiment may have been due to surface effects in the mixing bulb. It was also found that the F_B value slowly increased with time for a given reaction bulb mixture, doubling in value approximately every 9 hours. The F_B value was also found to go well beyond the predicted equilibrium value at 348K.

Although there was a great deal of uncertainty in the data, analysis of the Reaction (2) rate constant was performed.

A linear regression was used to fit the methane-iodine log k_{40} results. A line with a positive slope, which would correspond to a reaction with a negative activation energy, was found to be $\log k_{40}\ (cm^3/mole\ sec) = 6.71 + 0.719\ (\frac{10^3}{T}) \pm 1.4$. The same technique was applied to the methane-oxygen-iodine results. A second line, which also had a positive slope, was found to be $\log k'_{40}\ (cm^3/mole\ sec) = 7.72 + 0.0345\ (\frac{10^3}{T}) \pm 1.4$. Because of the large scatter in the data, the linear-correlation coefficients were quite low.

The experiments with oxygen present in the reaction mixture showed a slight increase in the rate of methyl iodide formation over the experiments performed in the absence of oxygen. Although this increase was less than the overall experimental error, an attempt was made to evaluate k_2. By use of Equation [75], the least squares fits of the methane-iodine and methane-oxygen-iodine data given above, and the oxygen-iodine ratio and T_5 reaction temperature determined in Experiment 14 of Table 10, the following estimation of the Reaction (2) rate constant was obtained:

$$k_2 = 5.4 \times 10^6 \text{ cm}^3/\text{mole sec.}$$

Of course, because of the large standard deviations in the rate constant data, this result is no more than a crude estimate of the upper limit of the Reaction (2) rate constant.

The theoretical value of k_2 estimated by Fristrom and Westenberg (53) at 1033K is 2.3×10^2 $\text{cm}^3/\text{mole sec}$, well below the upper limit determined in this work. The high rate of Reaction (40), under the above reaction conditions, limited the sensitivity of the experiment to the oxygen effect.

The log k_{40} and log k'_{40} data below 950K were considered invalid, due to the effects of the experimental and analytical errors described above. Thus, only taking data points above 950K and with the exclusion of the "anomalous" datum from Experiment 7 of Table 9, the linear regressions were recalculated. Justification for these assumptions will be discussed later in the text. The fourteen remaining data points from Table 9 yielded log k_{40} ($\text{cm}^3/\text{mole sec}$) = $12.0 - 4.78 \left(\frac{10^3}{T}\right) \pm 3.3$, and the eight remaining data points from Table 10 yielded log k'_{40} ($\text{cm}^3/\text{mole sec}$) = $13.8 - 6.38 \left(\frac{10^3}{T}\right) \pm 3.1$. A recalculation of k_2, again by use of Experiment 14 from Table 10, yielded:

$$k_2 = 3.1 \times 10^6 \text{ cm}^3/\text{mole sec.}$$

The reduced data set yielded much larger regression coefficients, but the fewer number of data points resulted in larger standard deviations. The pre-Arrhenius and activation energy parameters were

much closer to the low-temperature values determined by Goy and Pritchard (70) and Golden et al. (81). The recalculated k_2 value was nearly a factor of 2 lower with these reduced data sets.

The reduced data sets were also combined with the low-temperature data of Goy and Pritchard and Golden et al. and an additional set of linear regressions yielded the following rate constants:

$$\log k_{40}\ (cm^3/mole\ sec) = 14.5 - 7.40\ (\frac{10^3}{T}) \pm 0.21,$$

$$\log k'_{40}\ (cm^3/mole\ sec) = 15.1 - 7.73\ (\frac{10^3}{T}) \pm 0.19.$$

The Reaction (2) rate constant was recalculated to be $k_2 = 3.4 \times 10^6$ cm^3/mole sec. This result was essentially equal to the previous calculation of k_2. The extrapolated value of log k_{40} from the low-temperature data of Goy and Pritchard and Golden et al. was used in place of the value determined from the methane-iodine shock experiment and k_2 was calculated to be $k_2 = 4.3 \times 10^5$ cm^3/mole sec. This result was still three orders of magnitude greater than the theoretical calculation of Fristrom and Westenberg.

Mass-spectral Experiments

With the hope of further elucidating the cause(s) of the perplexing problems found in the data obtained by the radio-iodine technique, mass-spectral analysis of the shocked and mixing bulb samples from an additional set of methane-iodine, and methane-oxygen-iodine experiments was attempted.

Samples taken for analysis were obtained by simply allowing the shocked sample in the reaction end of the shock tube, closed off by the ball valve, to expand into a 100 ml sample bulb attached to the unused outlet on the vacuum manifold, see Figures 10 and 12. The mixing-bulb samples were obtained by allowing the gas in the mixing bulb to expand through the re-evacuated ball-valve end section into a second 100 ml sample bulb. These samples were then taken for mass-spectral analysis.

Results from the mass-spectral experiments are given in Table 11. The first three experiments were carried out in the absence of oxygen. The last four experiments were performed with oxygen present in the reaction mixture.

The relative sensitivity for methyl iodide to methane was determined to be 1 to 2, thus equal concentrations of methyl iodide and methane would give a ratio of mass-spectral peak heights equal to 0.5, (i.e., methyl iodide, mass 142, divided by methane, masses 15 and 16).

The mass-spectral data were scattered about the extrapolated low-temperature results of Goy and Pritchard (70) and Golden et al. (81).

The data fell within the error of the extrapolated low-temperature results, except in Experiment 5 of Table 11 where the datum point was slightly below the error bar, and in Experiment 4 the result was slightly above the error bar.

The degree of scatter found in the mass-spectral data was of the same order of magnitude as the scatter found in the radio-iodine experiments. This scatter indicated that the region 5 shock conditions were subject to significant error.

Ethane, ethyl iodide and methylene iodide were not found in the mass-spectral analysis of both the shocked and mixing-bulb samples from the methane-iodine experiments. Oxygen was never found in any of the methane-iodine samples.

Likewise, in the methane-oxygen-iodine experiments, ethane, ethyl iodide and methylene iodide were never found. Additional species, such as hydrogen peroxide, carbon monoxide and higher molecular weight iodides, were never detected. The hydrogen peroxide and carbon monoxide peaks had high backgrounds; thus, sensitivity to these species was limited.

Methyl iodide was always detected in both the shocked and mixing-bulb samples. The shocked sample always showed a greater amount of methyl iodide than the mixing-bulb sample. The low-temperature experiments, numbers 3 and 4 of Table 11, yielded values within the experimental error, and although these values were on the high side of the extrapolated low-temperature line, these points were well below the values of log k_{40} and log k'_{40} determined in the previous radio-iodine experiments.

Formaldehyde was not detected in the first three methane-oxygen-iodine mass-spectral experiments; but in Experiment 7 of Table 11, the mass 30 peak of the shocked sample was significantly greater than the mass 30 peak of the mixing bulb (which was slightly greater than the mass 30 found in the background). The increase in the shocked-sample mass 30 peak was attributed to the formation of formaldehyde. The slight increase in mass 30 found in the mixing bulb sample, which was

found in each of the previous methane-oxygen-iodine and methane-iodine samples, was attributed to the elution of mass 30 from the walls of the spectrometer. The mass spectrometer had a very large background at mass 18, thus, it was not possible to determine the amount of water in the reaction samples.

Within the error of the determination, it was found that the mixing-bulb and shocked samples' methane and oxygen concentrations remained unchanged. Iodine and hydrogen iodide reacted with the copper walls of the spectrometer vacuum manifold and were never detected.

The absence of ethane, and ethyl iodide from the mass spectrum eliminated Reaction (48) as a possible explanation for the apparent lack of increase in the rate of Reaction (40) with temperature. This will be discussed in greater detail later in the text.

The methyl iodide found in the mixing bulb, with the mass-spectral technique, was always less than the amount of methyl iodide found in the shocked sample. This result qualitatively supported the radio-iodine results; but the low-temperature results of the mass-spectral analysis indicated that the radio-iodine technique was quantitatively incorrect. Thus, the radio-iodine technique was suitable for large amounts of conversion of reactants to products, where the apparent, inherent degree of error in the determination of the fraction of reaction was relatively less important. Additional mass-spectral experiments would be required to confirm this result.

The results of the methane-iodine experiments supported the reported mechanism of Flowers and Benson (69). The validity of the

approximate solution to the rate equations for the formation of methyl iodide given by Equation [74] was confirmed by the absence of ethane and the low methyl iodide concentrations found in the shocked samples.

The lack of formation of formaldehyde coupled with the apparent absence of consumption of oxygen substantiated the approximate solution to the rate Equations for the methane-oxygen-iodine mechanism given by Equation [75].

The ratio of oxygen to iodine ranged between 0 and 4 for all but the final experiment in Table 11. The oxygen to iodine ratio for this experiment was 16.6 to 1. This was the only experiment in which formaldehyde was found.

The mass-spectral technique was well suited for these experiments. The background in the mass 142 region was negligible, the methyl iodide was readily ionized to CH_3I^+, and the technique did not require the purchase of expensive, short-lived iodine-131.

The data from Experiments 1, 2 and 3 of Table 11 were combined with the fourteen results from the methane-iodine high-temperature radio-iodine experiments and with the low-temperature results of Goy and Pritchard (70) and Golden et al. (81), and a linear regression was performed on this combined set of data. The Arrhenius parameters obtained for k_{40} were $A = 10^{14.5\pm0.19}$ cm^3/mole sec and $E = 33.7 \pm 0.64$ kcal/mole. Experiments 4, 5, 6 and 7 from Table 11 were combined with the eight results from the methane-oxygen-iodine high-temperature radio-iodine experiments and with the low-temperature results of Goy and Pritchard and Golden et al., and a linear regression was carried

out on this collection of data. The Arrhenius parameters obtained for k'_{40} were $A = 10^{14.9\pm0.24}$ cm^3/mole sec and $E = 34.8 \pm 0.48$ kcal/mole.

By use of the data from Experiment 7 of Table 11, the least squares fit for k_{40} and k'_{40} from the combined data sets and Equation [75], the following value for the upper limit of Reaction (2) rate constant was obtained:

$$k_2 = 9.53 \times 10^5 \text{ cm}^3\text{/mole sec.}$$

This value for k_2 is lower than the result from Experiment 14 of Table 10, obtained from the combined radio-iodine and low-temperature data sets, by a factor of 3. Thus, it is concluded that within the error of the experiment, at 1097K and with a stoichiometric methane-oxygen reaction mixture, Reaction (2) was not found to occur in this experiment.

The Arrhenius parameters obtained from the combined set of methane-iodine data were within the error of determination of the values obtained from the low-temperature work of Goy and Pritchard (70) and Golden et al. (81), as were the Arrhenius parameters obtained from the combined methane-oxygen-iodine data sets, see Table 12.

Table 12. Experimentally determined rate-constant parameters for Reaction (40) in cm^3, mole, sec, kcal units

Source	log A	E	Details
References (70) and (81)[a]	15.1 ± 0.53	35.5 ± 1.4	Temperature range was 549 to 629K. Total of 17 data points
This work CH_4-I_2 data[a]	14.5 ± 0.19	33.7 ± 0.64	Fourteen radio-iodine data points from 950 to 1151K, plus three mass-spectral data points from 859 to 1128K, plus data from References 70 and 81
This work CH_4-O_2-I_2 data[b]	14.9 ± 0.24	34.8 ± 0.48	Eight radio-iodine data points from 950 to 1143K, plus four mass-spectral data points from 833 to 1176K plus data from References 70 and 81

[a]This result corresponds to k_{40} in the text.

[b]This result corresponds to k'_{40} in the text.

The k_{40} and k'_{40} Arrhenius parameters are within the experimental uncertainty of each other. The shock-tube data, alone, have too large of an error to allow for a meaningful determination of Arrhenius parameters. Justification for the rejection of portions of the shock-tube data is appropriate at this time.

The low-temperature shock-tube results were rejected on the basis that the radio-iodine technique had a large background and a large uncertainty in a region where F_{rxn} should have been quite low. Also, the two mass-spectral low-temperature data points were far below the corresponding radio-iodine results, and thus supported the assumption that the radio-iodine low-temperature results were invalid.

The rejection quotient, Q, tabulated at the 90% confidence level in Skoog and West (77, p. 45) was used for critical examination of the outlying high-temperature results, namely Experiments 3 and 7 of Table 9. The Q test was also applied to the log k'_{40} result from Experiment 5 of Table 11.

Q test is designed for application to replicate analysis of a given sample. Of course, this requirement cannot be met with the shock-tube data, yet an approximation of "replicate samples", for the sake of this analysis, has been assumed to occur in rate determinations which were obtained at nearly equal temperatures. Thus, the data from Tables 9, 10 and 11 were lumped together into one large data set. The first experimental datum subjected to the Q test was Experiment 7 of Table 9. The high-temperature values near to Experiment 7 were taken from Experiment 22 of Table 9 and Experiment 7 of Table 11. The Q value

obtained was 0.95, which was greater than the 0.94 value quoted in Skoog and West, thus the measurement was rejected. Experiment 3 of Table 9 was compared with Experiments 2 and 6 of Table 9 and a Q value of 0.18 was obtained, thus this measurement was retained. Examination of the outlying result from Experiment 5 of Table 11, by comparison with Experiment 19 of Table 9 and Experiment 6 of Table 10, yielded a Q value of 0.68, thus this data point was retained.

Objections to the use of the Q test have been raised in the past, and certainly the validity of the use of the Q test presented here is exceedingly suspect. Nonetheless, the Q test did provide a crude justification for the rejection of the first high-temperature measurement.

Since ethane was never detected in any of the mass-spectral experiments, an estimation for the upper limit of Reaction (48) was made. The minimum concentration of ethane detectable was two units of peak height. The relative sensitivities for ethane and methane were estimated to be 14 and 8, respectively, by use of the theoretical values provided by Otvos and Stevenson (84). By use of the data from Experiment 2 of Table 11, the upper limit for the Reaction (48) rate constant was estimated to be:

$$k_{48} = 5.2 \times 10^3 \text{ cm}^3/\text{mole sec.}$$

This value is much too low to account for the "apparent" disappearance of product at high temperatures as was mentioned previously.

The Reaction (4) rate of formaldehyde formation calculated by use of Equation [78], the k_{41} rate constant value given in Table 7 and the data from Experiment 7 of Table 11, was found to be:

$$k_4 = 3.96 \times 10^{10} \text{ cm}^3/\text{mole sec.}$$

The relative sensitivities of methyl iodide to formaldehyde was assumed to be 3 to 1 by use of the theoretical values reported by Otvos and Stevenson (84). The estimated value of the Reaction (4) rate constant reported by Olson and Gardiner (13) at 1097K is 1.12×10^{10} cm^3/mole sec. Thus, the experimental measurement of k_4 reported in the present work supported the rate-constant value determined by Olson and Gardiner. In addition, the result reported for k_4 in this work was in disagreement with the 1220K upper limit of 3×10^8 cm^3/mole sec reported by Baldwin and Golden (62) and the high-temperature shock-tube study of Bhaskaran et al. (60) in which k_4 was estimated to be 5.5×10^7 cm^3/mole sec at 1097K.

CONCLUSION

The technique presented in this work has proven to be very useful in the study of several reactions. The rate constant value for Reaction (40) was extended to higher temperatures. The simple chain mechanism proposed by Flowers and Benson (69) for the free radical formation of methyl iodide and hydrogen iodide from methane and iodine was supported. The initiation reaction between methane and oxygen in a stoichiometric reaction mixture at 1097K was not found to occur. Finally, the measured rate of formaldehyde formation confirmed the low activation energy mechanism for methyl radical-oxygen reaction.

There is potential for other interesting and important results to be obtained from this technique. It is recommended that future experiments make use of the mass-spectral analytical technique. Additional methane-iodine experiments would be useful for improvement of the Arrhenius parameters for Reaction (40) determined from the shock-tube studies and for calibration of the overall experimental error. High-temperature studies, e.g., up to 1400K on methane-oxygen-iodine or methyl iodide-oxygen-iodine mixtures, would be useful in the study of the methane-oxygen initiation reaction and in the further elucidation of the mechanism of formaldehyde formation. Addition of known amounts of diazomethane (see for example, Glänzer et al. (85)), and/or methyl iodide to the methane-iodine reaction mixture would be useful for the study of the proposed overall chain-mechanism model. Addition of known amounts of diazomethane and/or formaldehyde to the

methane-oxygen-iodine reaction mixtures would provide a means to investigate the details of the model proposed for this system.

Fundamentally, it appears that whenever iodine atoms are present in a hydrocarbon mixture, the abstraction of hydrogen from C-H bonds will occur. In addition, the reactions of free radicals (formed, for example, by the loss of a hydrogen atom from a hydrocarbon) in the presence of iodine results in the rapid formation of R-I bonds. Thus, the iodine-iodine atom system provides a means for the steady formation of free radicals followed by efficient, rapid quenching of the product species.

According to Lewis and von Elbe (86), the addition of small amounts of iodine or methyl iodide to hydrogen-oxygen, oxygen-carbon monoxide, and methane-air reaction mixtures effectively suppresses explosive and slow reactions, and has a profound effect on the mechanism of the combustion process.

LITERATURE CITED

1. Benson, S. W. "Foundations of Chemical Kinetics"; McGraw-Hill: New York, 1960; Page viii.

2. Golden, D. M. J. Phys. Chem. 1979, 83, 108.

3. Gardiner, W. C., Jr. Acc. Chem. Res. 1977, 10, 326.

4. Olson, D. B.; Tanzawa, T.; Gardiner, W. C., Jr. Int. J. Chem. Kin. 1979, 11, 23.

5. Tsuboi, T.; Wagner, H. G. Symp. (Int.) Combust. [Proc.] 1975, 15, 883.

6. Westbrook, C. K. Combust. Sci. Technol. 1979, 20, 5.

7. Skinner, G. B.; Lifshitz, A.; Scheller, K.; Burcat, A. J. Chem. Phys. 1972, 56, 3853.

8. Heffington, W. M.; Parks, G. E.; Sulzmann, K. G. P.; Penner, S. S. Symp. (Int.) Combust. [Proc.] 1977, 16, 997.

9. Glass, G. P.; Kistiakawsky, G. B.; Michael, J. V.; Niki, H. Symp. (Int.) Combust. [Proc.] 1965, 10, 513.

10. Gardiner, W. C., Jr.; Olson, D. B. Ann. Rev. Phys. Chem. 1980, 31, 377.

11. Hartig, R.; Troe, J.; Wagner, H. G. Symp. (Int.) Combust. [Proc.] 1971, 13, 147.

12. Troe, J.; Wagner, H. G. Ber. Bunsenges. Phys. Chem. 1967, 71, 937.

13. Olson, D. B.; Gardiner, W. C., Jr. Combust. Flame 1978, 32, 151.

14. Brabbs, T. A.; Brokaw, R. S. Symp. (Int.) Combust. [Proc.] 1975, 15, 893.

15. Schecker, H. G.; Jost, W. Ber. Bunsenges. Phys. Chem. 1969, 73, 521.

16. Westenberg, A. A.; de Haas, N. J. Phys. Chem. 1972, 76, 2213.

17. Bowman, C. T. Symp. (Int.) Combust. [Proc.] 1975, 15, 869.

18. Lloyd, A. C. Int. J. Chem. Kinet. 1974, 6, 169.

19. Westbrook, C. K.; Creighton, J.; Lund, C. J. Phys. Chem. 1977, 81, 2542.

20. Zellner, R.; Steinert, W. Int. J. Chem. Kin. 1976, 8, 397.

21. Roth, P.; Just, Th. Ber. Bunsenges. Phys. Chem. 1975, 79, 682.

22. Roth, P.; Just, Th. Ber. Bunsenges. Phys. Chem. 1977, 81, 572.

23. Baulch, D. L.; Drysdale, D. D.; Horn, D. G. Symp. (Int.) Combust. [Proc.] 1973, 14, 107.

24. Baulch, D. L.; Drysdale, D. D.; Horn, D. G. "Evaluation of Kinetic Data for High Temperature Reactions"; Butterworths: London, 1973; Vol. 1-5.

25. Clark, T. C.; Izod, T. P. J.; Kistiakowsky, G. B. J. Chem. Phys. 1971, 54, 1295.

26. Lin, M. C.; Back, M. H. Canad. J. Chem. 1966, 44, 2357.

27. Baldwin, R. R.; Simmons, R. F.; Walker, R. W. Trans. Faraday Soc. 1966, 62, 2468.

28. Schofield, K. Planet. Space Sci. 1967, 15, 643.

29. Benson, S. W.; Haugen, G. R. J. Phys. Chem. 1967, 71, 1735.

30. Vandooren, J.; Tiggelen, P. J. Symp. (Int.) Combust. [Proc.] 1977, 16, 1133.

31. Creighton, J. R. J. Chem. Phys. 1977, 81, 2520.

32. Tsuboi, T. Jpn. J. Appl. Phys. 1976, 15, 159.

33. Asaba, T.; Yoneda K.; Kakihara, N.; Hihita, T. Symp. (Int.) Combust. [Proc.] 1963, 9, 193.

34. Miyama, H.; Takeyama, T. J. Chem. Phys. 1964, 40, 2049.

35. Terao, K. J. Phys. Soc. (Japan) 1960, 15, 2086.

36. Higgin, R. M. R.; William, A. Symp. (Int.) Combust. [Proc.] 1969, 12, 579.

37. Soloukhin, R. I. Symp. (Int.) Combust. [Proc.] 1967, 11, 671.

38. Voevodskii, V. V. Proc. Acad. Sci. USSR Phys. Chem. Sect. 1965, 161, 315.

39. Skinner, G. B.; Rührwein, R. A. J. Phys. Chem. 1959, 63, 1736.

40. Bowman, C. T. Combust. Sci. Technol. 1970, 2, 161.

41. Miyama, H.; Takeyama, T. Bull. Chem. Soc. (Japan) 1965, 38, 37.

42. White, D. R. Contract AF 33(615)-5772 Rep. S-70-1054 OARS Wright-Patterson Air Force Base; Dayton, Ohio.

43. Seery, D. J.; Bowman, C. T. Combust. Flame 1970, 14, 32.

44. Bowman, C. T.; Seery, D. J. Combust. Flame 1968, 12, 611.

45. Dryer, F.; Naegeli, D.; Glassman, I. Combust. Flame 1971, 17, 270.

46. Dryer, F.; Glassman, I. Symp. (Int.) Combust. [Proc.] 1973, 14, 987.

47. Baulch, D. L.; Drysdale D. D. Combust. Flame 1974, 23, 215.

48. Simmonaitis, R.; Heicklen, J. J. Chem. Phys. 1972, 56, 2004.

49. Homer, J. B.; Hurle, I. R. Proc. Roy. Soc. (London) 1970, A314, 585.

50. Tabayashi, K.; Bauer, S. H. Combust. Flame 1979, 34, 63.

51. Cullis, C. F.; Hinshelwood, C. N. Discuss. Faraday Soc. 1974, 2, 117.

52. Semenov, N. N. "Some Problems in Chemical Kinetics and Reactivity"; Princeton University Press: Princeton, N.J., 1959; Vol. II, Chap. XII.

53. Fristrom, R. M.; Westenberg, A. A. "Flame Structure"; McGraw-Hill: New York, 1965; Page 341.

54. Denisov, E. T. Russ. J. Phys. Chem. 1964, 38, 1.

55. Ernst, J.; Wagner, H. G.; Zellner, R. Ber. Bunsenges. Phys. Chem. 1978, 82, 415.

56. Peeters, J.; Mahnen, G. Symp. (Int.) Combust. [Proc.] 1973, 14, 133.

57. Reitel'boim, M. A.; Romanovich, L. B.; Vedeneev, B. I. Kinet. Catal. 1978, 19, 1131.

58. Skinner, G. B. "Introduction to Chemical Kinetics"; Academic Press: New York, 1964; Page 76.

59. Basco, N.; James, D. G. L.; James, F. C. Int. J. Chem. Kinet. 1972, 4, 129.

60. Bhaskaran, K. A.; Frank, P.; Just, T. Symp. (Int.) Shock Tubes Waves [Proc.] 1980, 12, 503.

61. Washida, N.; Bayes, K. D. Int. J. Chem. Kinet. 1976, 8, 777.

62. Baldwin, A. C.; Golden, D. M. Chem. Phys. Lett. 1978, 55, 350.

63. Klais, O.; Anderson, P. C.; Laufer, A. H.; Kurylo, M. J. Chem. Phys. Lett. 1979, 66, 598.

64. Izod, T. P. J.; Kistiakowsky, G. B.; Matsuda, S. J. Chem. Phys. 1971, 55, 4425.

65. Clark, T. C.; Izod, T. P. J.; Matsuda, S. J. Chem. Phys. 1971, 55, 4644.

66. Jachimowski, C. J. Combust. Flame 1974, 23, 233.

67. Zaslonko, I. S.; Smirnov, V. N. Kinet. Catal. 1979, 20, 470.

68. Potsuma, M. L. In "Free Radicals"; Kochi, J. D., Ed.; John Wiley and Sons: New York, 1973; Vol. II, Chap. 15.

69. Flowers, M. C.; Benson, S. W. J. Chem. Phys. 1963, 38, 882.

70. Goy, C. A.; Pritchard, H. O. J. Phys. Chem. 1965, 69, 3040.

71. Saito, K.; Tahara, H.; Kondo, O.; Yokubo, T.; Higashihara, T.; Murakami, I. Bull. Chem. Soc. (Japan) 1976, 49, 965.

72. Britton, D.; Davidson, N.; Schott, G. Discus. Faraday Soc. 1954, 17, 58.

73. Blake, J. A.; Burns, G. J. Chem. Phys. 1971, 54, 1480.

74. Kassman, A. J. "Kinetics of Methyl Iodide-Iodine Exchange in a Shock Tube", Unpublished Ph.D. Dissertation, Iowa State University, Ames, Iowa.

75. JANAF Thermochemical Tables, Thermal Research Laboratory, Dow Chemical Company, Midland, Michigan, 1970.

76. Bowman, C. T.; Hanson, R. K. J. Phys. Chem. 1979, 83, 757.

77. Skoog, D. A.; West, D. M. "Fundamentals of Analytical Chemistry", 2nd ed.; Holt, Rinehart and Winston, Inc.: New York, 1969; Page 455.

78. Harris, G. M.; Willard, J. E. J. Am. Chem. Soc. 1954, 76, 4678.

79. Scarborough, J. B. "Numerical Mathematical Analysis", 5th ed.; Johns Hopkins Press: Baltimore, Maryland, 1962; Page 356.

80. Gear, W. C. "Numerical Initial Value Problems in Ordinary Differential Equations"; Prentice-Hall, Inc.: Englewood Cliffs, New Jersey, 1971; Chap. 11.

81. Golden, D. M.; Walsh, R.; Benson, S. W. J. Am. Chem. Soc. 1965, 87, 4053.

82. Bevington, P. R. "Data Reduction and Error Analysis for the Physical Sciences"; McGraw-Hill Inc.: New York, 1969; Chap. 6 and 7.

83. Moore, W. J. "Physical Chemistry", 4th ed.; Prentice-Hall, Inc.: Englewood Cliffs, New Jersey, 1972; Page 57.

84. Otvos, J. W.; Stevenson, D. P. J. Am. Chem. Soc. 1956, 78, 546.

85. Glänzer, K.; Quack, M.; Troe, J. Symp. (Int.) Combust. [Proc.] 1977, 16, 949.

86. Lewis, B.; von Elbe, G. "Combustion, Flames, and Explosions of Gases", 2nd ed.; Academic Press Inc.: New York, 1961; Pages 70, 89 and 320.

ACKNOWLEDGEMENTS

First of all, I would like to thank Dr. Don S. Martin for patiently working through this problem with me.

I would also like to thank Gerald Flesch and Dr. Harry J. Svec for their assistance in obtaining mass-spectral data.

I thank Mike Rodgers for his comments and advice on the principles of composition.

I thank my good friends, Carey and Jean Johnson, Rich Tamura and Keith Schrag for the support, encouragement and kindness that they shared with me throughout my time at Iowa State University.

Finally, and most importantly, I thank Almighty God for the discipline and love that He gave to me so that I might complete this task.